CAPTURING DYNAMIC SCAFFOLD PROPERTIES OF HYBRID GELMA BASED MICROGELS TOWARD TISSUE ENGINEERING AND ORGAN-ON-CHIPS

A THESIS SUBMITTED TO

THE GRADUATE SCHOOL OF ENGINEERING AND SCIENCE

OF BILKENT UNIVERSITY

IN PARTIAL FULFILLMENT OF THE REQUIREMENTS FOR

THE DEGREE OF

MASTER OF SCIENCE

IN

MATERIALS SCIENCE & NANOTECHNOLOGY

By

Aslı Gizem Çınar

September 2024

CAPTURING DYNAMIC SCAFFOLD PROPERTIES OF HYBRID GELMA BASED MICROGELS TOWARD TISSUE ENGINEERING AND ORGAN-ON-CHIPS

By Aslı Gizem Çınar

September 2024

We certify that we have read this thesis and that in our opinion it is fully adequate, in scope and in quality, as a thesis for the degree of Master of Science.

Bülend Ortaç(Advisor)

Gurkan Yesiloz(Co-Advisor)

Işıl Gerçek Beşkardeş

Aykut Erbas

Approved for the Graduate School of Engineering and Science:

Orhan Arikan
Director of the Graduate School

ABSTRACT

CAPTURING DYNAMIC SCAFFOLD PROPERTIES OF HYBRID GELMA BASED MICROGELS TOWARD TISSUE ENGINEERING AND ORGAN-ON-CHIPS

Aslı Gizem Çınar
M.S. in Materials Science & Nanotechnology
Advisor: Bülend Ortaç
Co-Advisor: Gurkan Yesiloz
September 2024

Microgels have emerged as versatile materials in tissue engineering, drug delivery, and organ-on-chip (OoC) platforms due to their small scale, uniformity, and customizable properties. Their adaptability as injectable materials and dynamic scaffolds makes them promising candidates for a wide range of biomedical applications. However, traditional methods for characterizing their physical and mechanical behaviors, designed for bulk hydrogels, do not capture the unique properties of microgels, which differ significantly in terms of size and surface-to-volume ratio.

This work explores the physical properties of Gelatin Methacryloyl (GelMA)-based Collagen and Hyaluronic Acid Methacrylate (HAMA) hybrid microgels produced via droplet microfluidics, employing novel assays tailored specifically to their micro-scale. Real-time observation of their swelling and degradation properties is carried out using a custom-made platform enabling the tracking of individual microgels, and electron microscopy provides insights into their internal structures, revealing previously unobserved behaviors. We have shown the interpenetrating network formation when GelMA and Collagen are used; and copolymer formation when GelMA and HAMA are used. Under the effect of Collagenase and Hyaluronidase, the individual microgels showed different degradation mechanisms, which have proven to be affected by crosslink densities, enzyme-substrate specificity, enzyme saturation, and properties of the individual network components. The work is extended by focusing more on the temporal profiling of GelMA and HAMA hybrid microgels' behaviors under enzymatic degradation, examining how volume, mechanical properties, and surface features evolve over time, simulating the dynamic conditions encountered in vivo during especially tissue

engineering applications. We found that instead of carrying out separate assays to understand the changes, a more holistic approach to evaluating the aforementioned properties gives a more thorough discussion. This approach revealed that changing the ratios of GelMA against HAMA affects the crosslink densities, network formation, and ultimately degrative behaviors. We have observed, for the first time in droplet microfluidics, that a certain combination of GelMA HAMA results in microgels with a network gradient, getting denser towards the center, while the other combinations only increased the crosslink densities without altering the porous homogeneity. Furthermore, the number of microgels exposed to the same concentration of enzyme is altered to emulate different injection volumes into similar tissues, or the enzyme concentration is altered to emulate injection into different tissues. These assays showed the sensitivity of degradation profiles against enzyme saturation and competition. Meanwhile, the stiffness and surface morphology changes of microgels during degradation are examined, revealing the importance of network homogeneity in presenting stable mechanical properties during degradation. Lastly, drug release from these scaffolds is modeled for prospective applications, and their relation to scaffold properties is evaluated.

Overall, this thesis is poised to discover the peculiar behaviors of GelMA hybrid microgels produced with droplet microfluidics uncovering the importance of carrying out investigations true to the sample at hand and the conditions that will be imposed upon them during application.

Keywords: Biomaterials, Hydrogels, Microgels Organ-on-Chips, Tissue Engineering, Microfluidics, Enzymatic Degradation, Capillary Micromechanics .

ÖZET

DOKU MÜHENDISLIGI VE ÇIP-ÜSTÜ-ORGAN UYGULAMALARI IÇIN HIBRIT GELMA TABANL MIKROJELLERIN DINAMIK ORTAMLARDAKI ISKELET ÖZELLIKLERININ INCELENMESI

Aslı Gizem Çınar
Malzeme Bilimi ve Nanoteknoloji, Yüksek Lisans
Tez Danışmanı: Bülend Ortaç
İkinci Tez Danışmanı: Gurkan Yesiloz
Eylül 2024

Mikrojeller, geçtiğimiz yıllarda çip-üstü-organ platformları, doku mühendisliği, ve ilaç salınımı uygulamarında kullanışlıklıkları, özelleştirilebilir olamaları ve küçük boyutları ile önemlerini ispat etmişlerdir. Enjekte edilebilir malzemeler ve dinamik doku mühendisliği iskeletleri gibi farklı uygulamalara adapte olabilmeleri ile oldukça çeşitli biyomedikal aplikasyonlar için ümit vadedici platformlar olmuşlardır. Ancak, fiziksel ve mekanik karakterizasyonları için büyük ölçekli hidrojellerde kullanılan geleneksel metodların kullanılması, mikrojellere özel davranışların boyut ve yüzey alanına hacim oranının göz ardı edilerek yakalanamamasına neden olmaktadır.

Bu çalışmada, damlacık mikroakışkan çipler kullanılarak üretilen Jelatin Metakriloil (GelMA) tabanlı Kolajen ve Hyaluronik Asit Metakrilat (HAMA) hibrit mikrojelleri üretilerek, fiziksel özelliklerini araştırmak amacıyla mikro boyutlarına uygun olarak geliştirilen yeni nesil deneysel yaklaşımlar geliştirilmiştir. Şişme ve degrede olma özellikleri, bu amaca özel geliştirilmiş platformlar kullanılarak gerçek zamanlı bir şekilde takip edilmiş, iç yapıları taramalı electron microskopu kullanılarak aydınlatılmış, böylece daha önce raporlanmamış sonuçlar elde edilmiştir. Böylece, GelMA ve Kolajen kullanıldığında iç-içe geçen bir ağ yapısı gözlemlenirken, GelMA ve HAMA kullanıldığında kopolimer bir ağ yapısı gözlemlenmiştir. Kolajenaz ve Hyaluronidaz etkisi altında, bu mikrojeller ağ yapılarına, ağ yapılarının yoğunluğuna ve substrat-enzim etkileşimine, enzim doygunluğuna ve polimerlerin ağa bireysel katkılarına bağlı olduğu anlaşılan farklı degredasyon mekanizmaları göstermiştir. Çalışma, daha ziyade GelMA

ve HAMA hibrit mikrojellerinin vücut içerinde maruz kalacakları ortam taklit edilecek şekilde, enzimatik degredasyon altındaki davranışlarına odaklanarak genişletilmiş, hacimlerinin, mekanik ve yüzey özelliklerinin nasıl değiştiği incelenerek ilerletilmiştir.

Çalışmalarımız sonucunda bulduk ki, mikrojellerin geçirdiği değişimi anlamlandırabilmek için, bahsedilen deneylerin ayrı ayrı değerlendirilmesi yerine, bir bütün olarak değerlendirilmeleri sağlıklı çıkarımlar yapabilmek için daha faydalı olacaktır. Böyle bir yaklaşım benimsenerek, GelMA ve HAMA nın değişen oranlarının ağ yoğunluğunu, formasyonunu ve en nihayetinde degradasyon davranışlarını nasıl etkilediği aydınlatılmıştır. Çalışmamızda, damlacık mikroakışkan çiplerle üretilen mikrojellerde ilk kez gözlemlenen bir bulgu olarak, artan HAMA konsantrasyonlarında mikrojellerin merkezlerinden dışına doğru azalan bir ağ yoğunluğu bulunmuştur. Ayrıca, farklı enjeksiyon volümlerini taklit etmek amacıyla aynı enzim konsantrasyonunda farklı mikrojel sayıları degrede edilmiş, ve farklı enjeksiyon dokularını taklit etmek amacıyla, mikrojel sayıları sabit tutularak farklı enzim konsantrasyonları denenmiştir. Bu deneyler, mikrojellerin degredasyon profillerinin enzim doygunluğuna ve rekabetine karşı ne kadar hassas olduğunu göstermiştir. Bunlarla birlikte, mikrojellerin degredasyon sırasında sertliklerindeki ve yüzey özelliklerindeki değişim takip edilmiş, ağ homojenitesinin stabil bir sertlik değişimi profili çizmeleri için ne kadar önemli olduğu bulunmuştur. Son olarak, tüm bu bulguların mikrojellerin bir uygulaması olan ilaç salınımında nasıl bir etkisi olduğu edinilmiş bilgiler çerçevesinde değerlendirilmiştir.

Sonuç olarak, bu tez, damlacık mikroakışkan çip kullanılarak üretilen GelMA hibrit mikrojellerinin kendilerine has özelliklerinin keşfedilmesi için eldeki örneklerin boyutuna ve uygulamada kullanılacakları koşullara uygun olarak test edilmelerinin önemini apaçık bir şekilde vurgulamıştır.

Anahtar sözcükler: Biyomalzemeler, Hidrojeller, Mikrojeller, Çip-Üstü-Organ, Doku Mühendisliği, Mikroakışkanlar, Enzimatik Degredasyon .

Acknowledgement

I would like to begin by expressing my deepest gratitude to my supervisor, Assoc. Prof. Dr. Gürkan Yeşilöz. Words cannot fully capture how thankful I am for the role he has played in shaping not only my academic journey but also my personal growth. His support, insightful guidance, and generous mentorship have been invaluable. The knowledge and experiences I've gained under his supervision have laid a strong foundation for my future, I am a different person today than when I embarked on this path, and it is clear that his influence has been a guiding light in that transformation. For that, I will be forever grateful. It has been a pleasure being part of his lab from its early days and seeing it become grown, renowned, and impactful. Thank you for making me a part of it.

Many thanks to my beloved lab members, the friends I have gained along the way, Dr. Munir, Eylül, Faruk, Ali, Faiqa, Ecem, and Servin; it was a pleasure to work with all of you, get to know you, and find laughter in our good and bad times. We have uplifted each other and taught each other many things.

I would like to thank my mom, Gülsün Çınar, who helped me see these days, my success is yours. My sister, Didem Çınar, thank you for being my sister (and my unofficial academic funder), and my nephew, Emir Can Seyhan; I'm not sure if you will ever see this, but here's to you, kiddo. And, of course, my cat, Ollie, for the times I forcefully hugged him to find comfort. And my dearest friend, Zeynep Köker, my comrade in academic troubles and personal growth, we have grown a lot, haven't we? Thank you for being by my side, filling my days with happiness, and helping me become a better version of myself.

In addition, I would like to acknowledge the generous financial support from the Scientific and Technological Research Council of Türkiye (TÜBİTAK) BIDEB International Outstanding Researchers Program under project No. 118C263 and ARDEB 1001 Program Under Project No. 221M575.

Overall, as Charles Dickens puts it, “It was the best of times, it was the worst of times, it was the age of wisdom, it was the age of foolishness, it was the epoch of belief, it was the epoch of incredulity, it was the season of light, it was the season of darkness, it was the spring of hope, it was the winter of despair.”

Also, last but not least:

Contents

List of Figures

List of Tables

Chapter 1

Introduction

1.1 Microgels and Their Characterizations for Tissue Engineering and Organ-on-Chip Applications

Microgels have been of great interest to biomedical sciences in recent years. With the benefits and opportunities coming with their small scale, they secured a prominent place in tissue engineering, drug delivery and lately in organ-on-chip applications. This wide range of applicability can be attributed to their highly customizable structure from both chemical and physical aspects. Rationally, the opportunity to fine-tune and alter the microgels for specific applications requires a comprehensive understanding of their chemistry as well as their physical attributes. Whilst investigation of their chemistry is irrespective of their shape and size, the opposite case is valid for examining their physical properties such as swelling and degradation. Because of their micron-size and increased surface to volume ratio, they exhibit altered behaviors compared to their bulk counterparts. However, assays being carried out to understand these attributes are mostly done on the bulk version of these microgels, which presents unrealistic results where swelling and degradation times take days, and pore sizes appear as big as the microgel itself. In this manner, there is a high need to present time efficient alternative assays to investigate the real time swelling, degradation and other structural analyses of these microgels on small scale.

The significance of analyzing microgel behaviors as accurately as possible can be realized with a close look into their applications. For instance, in tissue engineering, microgels have been of choice for providing support to cells in terms of increasing their viability through fast nutrient and waste transport [1, 2, 3, 4, 5]. In pharmaceuticals, they can be used as controlled drug delivery vehicles due to their alterable biodegradation rates and permeability [6, 7, 8, 9]. For Organ-on-chip (OoC) platforms on the other hand, on-chip cell-laden microgel production with a following on-chip incubation for spheroid, organoid or cell aggregate formation is desired for high-throughput drug evaluation assays and tissue

formation[10, 11, 12, 13]. In this manner, for such OoC implementations, examining the behavior of microgels in general, and their swelling and degradation profile, in particular, in the micro-channels is important to optimize the design parameters of the chip. Therefore, with a thorough understanding of the microgels' inner structure, their interactions with the solutes, and enzymatic or hydrolytic degradation profiles, they can be customized to harbor whichever characteristic is desired through the selection of material composition, polymerization technique, and production method.

The material choice in this regard, or rather the polymer choice, forms the backbone of this customization potential[14, 15, 16, 17, 18]. Microgels can be produced from various natural and synthetic materials such as PEG, Gelatin, Alginate, and Hyaluronic Acid in various ways. With the preferred polymerization technique, resulting hydrogels can be from one type of polymer or a combination of polymers that can bring together the desired characteristics. As a matter of fact, recent years have shown the successful utilization of hybrid hydrogels for various applications. For instance, so far Gelatin methacryloyl (GelMA) has been used as a common hydrogel for tissue engineering, 3D cell culturing and drug delivery[19, 20, 21]. These applications mostly took the benefits of GelMA providing cell attachment sites, biodegradation motifs, moderate stiffness and it being photo-crosslinkable. In recent times, however, to further enhance GelMA hydrogel properties, it has been combined with other polymers such as Collagen and Hyaluronic Acid Methacrylate (HAMA). With Collagen addition, the fibrillar structure that is important for cell proliferation, migration and differentiation can be restored [22, 23], and with Hyaluronic Acid Methacrylate (HAMA), closer mimicry of ECM, especially the cartilage tissue can be precisely achieved [24, 25, 26]. As such tailor-made hybrid hydrogels have become appealing for various biomedical applications, their in-depth characterizations in intact terms gain importance. The established assays for the examination of such hydrogels start with the fabrication of the specimen in bulk, which is usually on a centimeter (cm) scale. For instance, in swelling characterizations using bulk gel sample, the specimen is first weighted (before swelling weight (wt)), then submerged in the required buffer solution for hours to swell, followed by another round of weighing

(after swelling wt), and lyophilization to measure the dry weight. The ratio of these gives the commonly used swelling ratio. Similarly, for degradation assays, specimen gets submerged in an enzyme solution and is taken out of the buffer daily or in couple of hours to weight the undegraded hydrogel. Though these assays are practical for comparing different bulk hydrogels; for micron sized gels, it is yet not known if these implementations will hold.

1.2 Microgels or Hydrogel Microparticle Scaffolds (HMPs) as Tissue Engineering Scaffolds

Traditional hydrogels used in tissue engineering are bulky polymeric structures, minimum at the millimeter scale, and have porosity at the nanometer scale. This scaling makes cell infiltration, attachment, and interaction difficult and hinders solute transport, affecting tissue replacement rates and immune responses. The pore size within the hydrogel can be increased through various fabrication techniques, such as sacrificial materials, cryogelation, freeze-drying, and porogen leaching. [27, 28] While helpful, especially with injectable hydrogels, materials processed in the mentioned ways are either not injectable, have a predetermined shape, or require additional processes in vivo. Microgels or hydrogel microparticles (HMPs) are favored alternatives as injectable biomaterials for providing macropores in addition to nanopores, higher stiffness ranges, concave surfaces, and for being inherently shear thinning, regardless of the material choice [29, 30, 31]. They have been used to repair the brain after a stroke by injection to the stroke cavity [32], the peripheral nerves after an injury [33], to regenerate and fill cartilage and bone defects [34, 4, 35, 36], and aid in the healing of myocardial tissue after myocardial infarction[37].

Some of these fabrication methods compromise size and shape uniformity for large production numbers, while others do the opposite. Techniques such as fragmentation, electrohydrodynamic spraying, and batch emulsions can produce large quantities in a short amount of time but result in nonuniform products. More sophisticated techniques, such as droplet microfluidics and lithography, prioritize uniformity and fall short of production speed. Despite that, utilization of droplet microfluidics soared owing to the precise control over microgels and the range of complexity it can provide. The uniformity gains importance when the cell response is in question, where the size and shape of particles affect the cellular outcome[38], in addition to drug release, where size corresponds to how much drug

is encapsulated and released. Furthermore, the complex shapes droplet microfluidics provides, whether the layered droplets or compartmentalized Janus droplets, have been useful for applications requiring compound delivery. [39, 40, 41]

1.3 Microgel Scaffolds in Dynamic Environments for Tissue Engineering Applications

Tissue engineering involves complex dynamic processes in vivo, where the scaffold and cells interact in an evolving feedback loop. Upon implantation, the scaffold initially guides cellular behavior through its mechanical properties[42, 43, 44], topology[45], surface chemistry, and porosity[46], all of which play a critical role in directing cell attachment, migration, proliferation, and differentiation[47]. However, as tissue regeneration progresses, this relationship becomes reciprocal—cells actively remodel the scaffold while the scaffold undergoes degradation, particularly in the case of biodegradable polymers. As cells infiltrate the scaffold, they release signaling molecules, recruit immune cells, and secrete extracellular matrix components, which collectively alter the local environment. Concurrently, the scaffold's properties change due to hydrolytic or enzymatic degradation, leading to shifts in mechanical stiffness, porosity, and surface topology. This degradation-driven evolution provides cells with continuously changing environmental cues, influencing their behavior over time.[48] For instance, decreasing stiffness as the scaffold degrades may impact cell differentiation, while newly exposed surface chemistries can alter adhesion and signaling pathways. This interplay is particularly significant in regenerative applications where the scaffold's temporal changes align with the different phases of tissue healing—from the initial immune response to later stages of tissue formation—creating a scaffold that is not static but dynamically evolving to support each stage of tissue regeneration.

Profiling the temporal changes a scaffold undergoes due to cellular activity is essential for optimizing scaffold design and utilization in tissue engineering. Understanding how scaffold properties evolve during degradation allows for the creation of dynamic environments that better mimic the natural tissue healing process. For instance, depending on the mode of degradation, a scaffold's volume may decrease while stiffness remains constant, or stiffness and mass may decline while volume stays the same. In microgels, where directly capturing mass changes is challenging due to their small size, monitoring stiffness variations can reveal

correlations between volume and mass, indirectly indicating changes in polymer structure and porosity. Such holistic evaluation becomes especially important in designing scaffolds with temporally controlled degradation rates. By profiling these temporal changes in mechanical properties, porosity, and biochemical signals, researchers can design scaffolds that deliver targeted cues at optimal times, improving regenerative outcomes. This approach also extends to applications such as drug delivery, where scaffold degradation can be tuned for controlled and sustained release of therapeutics. Ultimately, leveraging the temporal evolution of scaffold properties allows for tissue engineering strategies that align scaffold behavior with the dynamic needs of regenerating tissues, leading to more predictable and successful clinical outcomes.

1.4 Objective of the Thesis

The main objective of this thesis is to investigate the physical properties of hybrid hyaluronic acid and collagen compositions of GelMA microgels, aiming to advance their utilization in tissue engineering and microphysiological systems. The first part of the thesis emphasizes the significance of scale-wise investigations, as the micron size of the microgels affects the swelling and degradation behaviors and gives new possibilities for carrying out other assays, such as observing the inner structures. The microgels comprise GelMA, HAMA, and Collagen, which are widely utilized natural polymers in tissue engineering and in vitro assays as scaffolds. Droplet microfluidics is utilized to produce monodisperse, size-tunable microgels. The study meticulously explores the swelling, enzymatic degradation, and porous structure of 5 different compositions of microgels comparatively. Microgels with 10% GelMA(w/v), 9.25%GelMA:0.75%HAMA, 8.75%GelMA:1.25%HAMA, 8.75%GelMA:1.25%Collagen, and 7.5%GelMA:2.5%Collagen compositions are produced in a droplet microfluidic chip with in situ photopolymerization followed by swelling and degradation assays carried out in custom-made microwell platforms and inner structure observations with SEM, together with a proposed one-step solvent cleaning method. Building on this foundation, another comparative study is conducted among microgels of three different GelMA:HAMA compositions to investigate the changes in their physical properties and mechanics during enzymatic degradation, especially targeting tissue engineering applications. The compositions included 9.25%GelMA:0.75%HAMA, 9%GelMA:1%HAMA, and 8.75%GelMA:1.25%HAMA. The research examines various aspects of degradation, such as volume loss, shape retention, and the impact of enzyme concentration and microgel quantity on degradation. Additionally, it investigates how the stiffness of individual microgels changes using the capillary micromechanics method, drug release profiles with model drugs (fluorescein, rhodamine B and congo red), and topological changes via light microscopy and SEM. As scaffold properties directly influence cell behavior, including proliferation, differentiation, and immune response, profiling their temporal changes is crucial.

Chapter 2

Investigating Physical Properties of Hybrid Hyaluronic Acid and Collagen Compositions of GelMA Microgels Toward Tissue Engineering and Organ-on-Chip Applications

Declaration of Copyright

This work is described in the following publication [49]

Asli Gizem Cinar 1,2, Iqra Munir 1 and Gurkan Yesiloz# 1,2

1 UNAM-National Nanotechnology Research Center, Bilkent University, 06800 Ankara, Türkiye

2 Institute of Materials Science and Nanotechnology, Bilkent University, 06800 Ankara, Türkiye

#Corresponding author: gurkan.yesiloz@bilkent.edu.tr or gurkan@unam.bilkent.edu.tr

Adapted from Cinar, A. G., Munir, I., & Yesiloz, G. (2023). Investigating Physical Properties of Hybrid Hyaluronic Acid and Collagen Compositions of GelMA Microgels toward Tissue Engineering and Organ-on-Chip Applications. *ACS Applied Polymer Materials*, *5*(10), 8121-8132.

2.1 Introduction

In this chapter, we propose a resolution to the restrictions coming from the size insensitivity towards microgels during characterization by analyzing the swelling, degradation, and structural analysis assays that are tailored for individual single microgels. For this, we have utilized hybrid design microgels to match the recent trends and showcase how microgels with different compositions can be precisely investigated to understand their behavior and to reveal previously unexplored observations and aspects. GelMA was our main polymer of choice, with Collagen and HAMA as hybrid components. Microgels production was carried out in a droplet microfluidic platform with specific optimizations needed to generate homogenous droplets. The synthesized microgels were then washed with isopropyl alcohol (IPA) to dry and remove the continuous oil phase, which takes place of the undesired process of lyophilization due to its effect on structural changes. Upon drying, the microgels were examined with SEM to reveal inner structures and detailings coming from different combinations of hybrid materials. At last, the physical characterizations like swelling and degradation profiles, in real-time, were observed in a custom-made micro-well platform for single microgels individually. Excitingly, this platform offered, for the very first time, to carry out real-time examinations of swelling and degradation behavior of individual microgels in an agreeable 3D version, with real-time statistics for each combination of gel materials. When the microgel behavior is examined thoroughly with these tailored methods, it is probable that their characteristics and behaviors peculiar to their size, under various conditions, can be observed and altered with precision to match desired applications.

2.2 Materials and Methods

2.2.1 GelMA and HAMA synthesis

For the synthesis of Gelatin Methacryloyl (GelMA) and Hyaluronic Acid Methacrylate (HAMA), both gelatin and hyaluronic acid (HA) were methacrylated separately with slight alterations to the previously described protocols [19]. Briefly, 10% Gelatin (w/v) was mixed with PBS under continuous stirring at 60°C until fully dissolved. After dissolution, different volumes of methacrylate (MA) (v/v) was added in a dropwise manner over the course of 2 hours (10 μL/10sec). The solution was left to react for 3 hours at 50°C followed by the addition of an equal volume of warm PBS to quench the reaction. To get rid of the unreacted MA and the by-products of the reaction (i.e., methacrylic acid), the solution was dialyzed against distilled water using 12-14 kDa dialysis membrane at 40°C for 5-7 days. Dialyzed products were kept at -80°C overnight and then lyophilized for a week.

For HA methacrylation, 1% HA (w/v) was dissolved in PBS with slow additions and continuous stirring for 24 hours at room temperature. After HA was fully dissolved, 5% MA (v/v) was added dropwise over the course of a few hours (10 μL/10secs) by keeping the pH between 7-10 with continuous addition of 5M NaOH at 4°C. After 3 hours of mixing, the solution was diluted with an equal volume of PBS and dialyzed against distilled water in a 12-14 kDa dialysis membrane at 4°C for 5-7 days. The solution was frozen at -80°C overnight and then lyophilized for 3-5 days. Both resulting products were kept at -20°C until further use.

2.2.2 Degree of Methacrylation of Gelatin and HA

Methacrylation of GelMA and HAMA were examined with ^{1}H NMR spectroscopy as described previously[50, 51]. For GelMA, 20 mg of GelMA and Gelatin (as control) were each dissolved in 1 mL of warm D_2O and the solutions were kept at

37°C until the measurements. For the quantification of the Degree of Methacrylation (DM), initially, gelatin and GelMA spectra were normalized with respect to the phenylalanine signal at 6.9-7.5 ppm, which is expected to depend on the concentration of gelatin and not be affected by MA. Then, the integral of peaks that belong to lysine methylene at 2.7-2.9 ppm was taken. This peak was expected to decrease with MA substitution, contrary to the peaks at 5.2-5.6 ppm and at 1.9 ppm, which belong to newly formed methacryloyl groups, which should appear and increase with the amount of substitution. The DM was calculated as follows:

$$\mathrm{DM_{GelMA}} = \left(1 - \frac{A(\text{Lysine Methylene of GelMA})}{A(\text{Lysine Methylene of Gelatin})}\right) \times 100$$

In the case of Hyaluronic Acid Methacrylate (HAMA), 5mg of HAMA and HA (as control) were each dissolved in 1 mL D_2O at room temperature. To calculate the Degree of Methacrylation (DM), a similar protocol was used for the GelMA. The peak at 1.9 ppm in HA that belongs to methyl protons was altered upon methacrylation, and new peaks formed at 1.5-2.0 ppm in HAMA spectra. The peak at 1.8 ppm that belongs to MA methyl protons and the peaks at 5.6 – 6.1 ppm showing the presence of methacrylate vinyl groups confirmed the substitution. DM was calculated as follows:

$$\mathrm{DM_{HAMA}} = \left(1 - \frac{A(\text{HA Methyl proton peak (1.9 ppm)})}{A(\text{MA Methyl proton peaks (5.6-6.1 ppm)})}\right) \times 100$$

2.2.3 Hydrogel Precursor Preparation

Hybrid and bare hydrogel precursors were prepared to have a final 10% (w/v) gel content in the working buffer solutions throughout the study, otherwise mentioned. Hence, bare GelMA hydrogel was prepared by adding 10% (w/v) lyophilized GelMA product to PBS at 37 °C, and in the case of hybrid gel precursor preparation GelMA+hybrid-component was prepared to be 10% (w/v) in total accordingly.

HAMA and GelMA hybrid solutions were prepared by varying the ratios of two components as 0.75% HAMA + 9.25% GelMA, and 1.25% HAMA + 8.75% GelMA. These solutions were prepared by initially dissolving HAMA in PBS under continuous stirring at room temperature. Then, solution temperature was raised to 37°C and GelMA was added and mixed until homogeneous solution was obtained.

Similarly, Collagen and GelMA hybrid solutions were also prepared in two different concentrations as 1.25% Collagen + 8.75% GelMA, and 2.5% Collagen + 7.5% GelMA. Unlike the HAMA-GelMA hybrid gel, Collagen was initially dissolved in 0.1% acetic acid in PBS buffer at 4°C and used as interpenetrating agent. The amount of acetic acid buffer to dissolve Collagen in was kept at minimum by observing the dissolution capacity of acetic acid gradually. In this manner, 14 μL of 0.1% Acetic acid buffer was used to dissolve 1mg of Collagen. After Collagen dissolution, PBS and GelMA were added and mixed until getting homogeneous gel precursor at 37°C. At last, 0.5% (w/v) Lithium phenyl-2,4,6-trimethylbenzoylphosphinate (LAP) photoinitiator was added in each polymer solutions, and mixed until fully dissolved.

2.2.4 Fabrication of the Microfluidic Device

The microfluidic device is consisted of a polydimethylsiloxane (PDMS) mold with the designed microchannels for droplet generation and transport, and a glass substrate carrying the mold. For the fabrication of microfluidic chips, SU-8 masters were fabricated on silicon wafers using the similar soft-lithography technique we used in our previous works [52, 53]. Briefly, in order to make PDMS replica molds, PDMS prepolymer was mixed at a 10:1 ratio of base to curing agent, degassed, and molded against the SU-8/silicon master and then cured at 95 °C for 2 h. The molds were then peeled off from the master, and fluidic access holes were made using a 1.5 mm biopsy punch. The PDMS mold was then treated with oxygen plasma at 100 W, 400 mTorr for 30 s and bonded to a glass substrate.

2.2.5 Droplet Microgel Production and Collection

Microgels are produced via the droplet microfluidic platform (chip) designed and fabricated for this study. The chip has mainly three regions: a droplet formation part, a serpentine section, and an outlet reservoir. Droplet generation part is composed of a flow focusing design connected to two inlets: one for the hydrogel precursor and one for the oil phase. Silicon oil (50 cSt) is used as the continuous phase. The chip is placed onto a microscope (Zeiss, Axio Observer 7 inverted microscope) which is equipped with an incubation system that is able maintain the incubation chamber at 37°C stable temperature. Syringe pumps are used to inject the gel and oil phases into the microfluidic device. One of the syringe pumps utilized to feed the gel precursor is placed in a custom-made incubator chamber to keep the gel temperature at 37°C. The whole setup is designed to maintain a smooth fluidic operation and prohibited the clogging of the tubings as well as channels of the chip due to variations in the temperature, fluctuations, etc. Precursor solutions are then fed to the chip at variable flow rates through syringe pumps, for each solution, and droplet formation is observed under the microscope. Once the desired size of microgels is obtained, the microgels are allowed to polymerize under a light source (405 nm, 350 mW/cm2) which is placed 2 mm above the serpentine portion of the chip. The polymerized (cross-linked) gels are then reached to the reservoir chamber and collected in an Eppendorf with a micropipette for further use.

To confirm the monodispersity of droplets, coefficient of variance (CV) was calculated as below:

$$\mathrm{CV}(\%) = \frac{\sigma_{\mathrm{microgel}}}{\mu_{\mathrm{microgel}}}$$

$$\sigma_{\mathrm{microgel}} = \text{St Standard Deviation of the distribution}$$

$$\mu_{\mathrm{microgel}} = \text{Mean of the distribution}$$

which was less than 2% showing that monodispersed droplets are obtained. Upon the collection, gels were washed with isopropanol alcohol(IPA) with three times of centrifugation to isolate the oil phase of the droplet microfluidics device.

2.2.6 Morphological Characterization of Microgels under Scanning Electron Microscope (SEM)

To observe the morphology, pore size, and crosslinking details of the microgels, bare-dried microgels after the washing step (not freeze-dried/lyophilized) were sputter coated with an ultrathin layer of gold/palladium and imaged under SEM. The samples were imaged as a whole and in intersections to visualize in-depth differences between bare GelMA and hybrid microgels. The gels were cut and sliced carefully using sharp needles to avoid pinching of the microgels. The SEM images were used for the analysis, and the pore sizes were presented as the average of the maximum and minimum pore diameters, as discussed in the results section below.

2.2.7 Custom-made Microwell Platforms

In order to perform the swelling and degradation analysis of microgels, a custom-made microwell platform was designed and fabricated through a 3D-printer. Since there is no data available in literature so far to examine the swelling and degradation of individual single microgels in microscale, our design has presented a valuable addition for such observations. Each reservoir of the platform has multiple wells, and well dimensions were arranged to accommodate only 1 microgel at a time to enable simultaneous observations of multiple microgels from same composition at once.

2.2.8 Swelling of Microgels

Using the micro-well platform described above, swelling assays were carried out for all gel compositions using dry microgels. After cautiously placing each microgel in a single micro-well, a drop of buffer solution was injected to the respective well with the help of a syringe (having a blind needle). Microgels were allowed to swell completely until the maxima was achieved. Proceeding to this, Volume

Fold Swelling and Volumetric Swelling ratio were calculated for each composition as follows:

$$\text{Volume Fold Swelling} = \frac{D_s}{D_o^3}$$

$$\text{Volumetric Swelling} = \frac{V_s - V_o}{V_o} \times 100$$

where D_s and D_o denotes the swollen microgel and initial microgel diameters, respectively. Likewise, and represents the swollen and initial volume of the microgels, respectively.

2.2.9 Enzymatic Degradation of Microgels

For the enzymatic degradation of hybrid microgels having Gelatin, Collagen and Hyaluronic acid, Collagenase and Hyaluronidase were used. The stock solution of each enzyme was prepared in PBS to have the final concentrations of 5 CDU/mL and 40 IU/mL for Collagenase and Hyaluronidase, respectively, for 1 CDU and 8 IU final assays to be used in the analysis. Similar to the swelling assay, the custom-made microwell platform was used to observe the degradation of microgels in real-time. After the complete swelling of the microgels as explained above, 200 µL of enzyme solution at 37°C was added to the reservoir, and microwell platform was placed into the incubation chamber of microscope which is maintained at 37°C.

After image acquisition, degradation was calculated in two different trends, i.e., volume loss and complete degradation time. If the microgels showed a volumetric degradation profile where they kept their spherical shape, volume loss was calculated as follows:

$$\text{Volume Loss (\%)} = \frac{V_0 - V_t}{V_0} \times 100$$

where V_0 shows swollen microgel volume at the beginning (time, t=0) while representing the microgel volume at later stages (t¿0).

If microgels did not show a volumetric degradation profile and dissipated randomly in the microwell, complete degradation times were determined by observation and monitoring continuously in real time.

2.3 Results and Discussion

2.3.1 Synthesis and Preparing Hybrid Hydrogel Precursors

Degree of methacrylation (DM) is an important parameter to design hybrid hydrogels like GelMA and HAMA, since it effects the amount of crosslinking and consequently the physical behaviors of gels such as porosity, water retention capacity and degradation rate[54]. During the synthesis, it is possible to alter the DM with the amount of MA added. However, the resulting DM should be kept under check to utilize the least amount of MA for the desired DM, since unreacted MA is potentially cytotoxic.

For this work, we desired to keep the DM of GelMA and HAMA at its maximum with the least amount of MA, and after determining this value we used it as a constant parameter throughout the work. Since GelMA was the main component of the microgels in the current study, additional importance was given to its methacrylation, with optimization steps of different amounts of MA (1%, 5%, 20%) added during the synthesis protocol. Out of these percentages, a maximum of 77% DM of GelMA was observed for 5% MA (v/v) (Figure 2.1a), and no further effect was observed upon the addition of more MA (Figure A.1). Thus, 5% MA consisting of GelMA was used for further experiments. Likewise, the degree of methacrylation (DM) was also calculated for HA using a similar approach. Interestingly, at 5% MA, DM for HAMA was found to be 97% for HAMA (Figure 2.1b). Hence, we did not analyze other concentrations of MA for HAMA gels.

After methacrylation, working solutions were prepared with different polymer concentrations of gel components (GelMA, Collagen, and HAMA) while keeping the total gel content at 10% (Table 1). The reason for fixing the total gel concentration as 10% was to be able to control the physical properties of microgels only with the hybrid addition and not with the amount of total polymer in the resulting gels, which also affects the overall hydrogel properties. For instance, with HAMA addition, the resulting microgels formed a copolymer network where

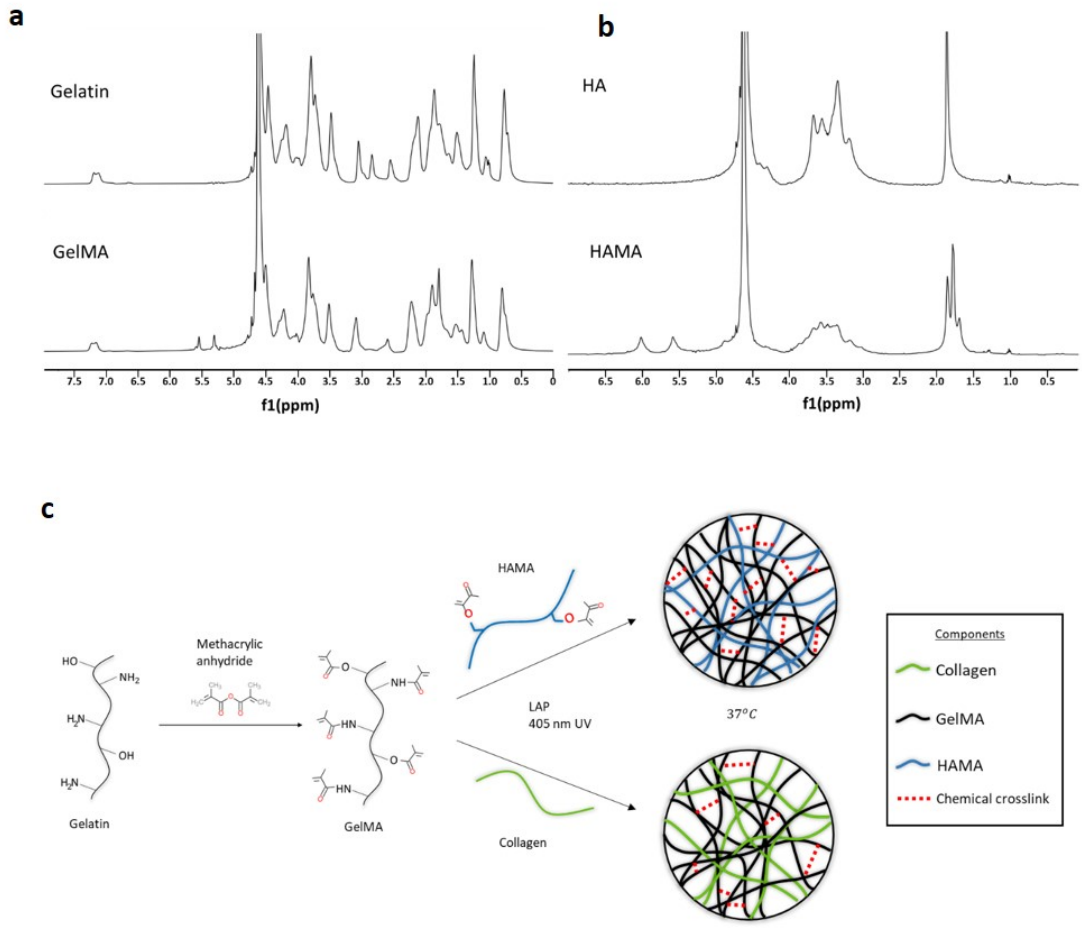

Figure 2.1: Synthesis and precursor solution preparation. ^{1}H NMR spectra of (a) Gelatin and GelMA, (b) HA and HAMA, (c) Methacrylation of GelMA and hybrid additions with subsequent photocrosslinking.

chemical crosslinking can occur among GelMA chains, HAMA chains, or between GelMA and HAMA chains[55].

Collagen addition, on the other hand, results in interpenetrating networks where chemical crosslinks form between methacryloyl groups of the GelMA chains, and physical crosslinks form between Collagen chains with the increase in temperature up to 37°C [23] (Figure 2.1c).

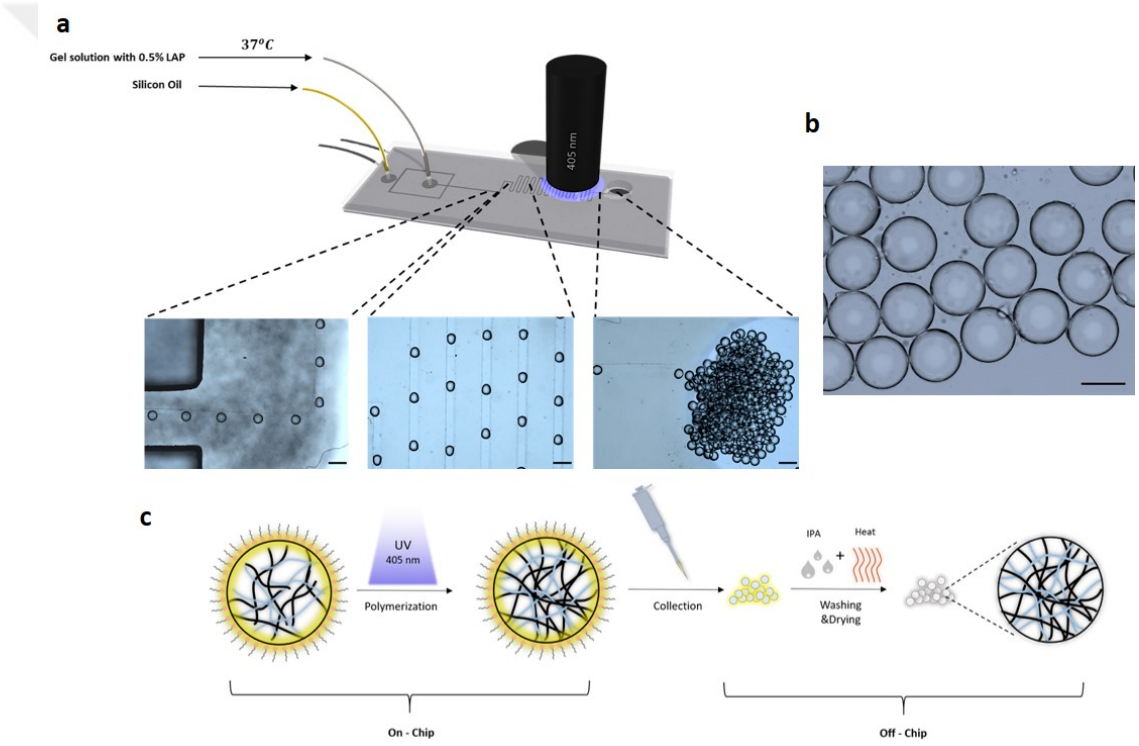

Figure 2.2: Microgel production schema. (a) Droplet microfluidic platform for microgels production and polymerization in situ. Scale bars: 500 μm. (b) Highly monodisperse microgels upon collection. Scale bar: 200 μm. (c) Collection, washing, and drying of gels for further characterization.

2.3.2 Microgel Production

With the aim of producing high throughput and monodispersed microgels, in this work, we utilized a droplet microfluidic platform coupled with a light source, thereby allowing one platform to be utilized for both production and polymerization of microgels at once (Figure 2.2a). For a better comparison of microgels with varying compositions, we preferred to keep the diameter of the microgels constant at 250 μm. To achieve the same droplet size with different gel precursors, the capillary number should be considered, which follows the relation below,

$$\mathrm{Ca} = \frac{\mu V}{\gamma}$$

where is the viscosity of the oil phase, V is the velocity of the oil phase and is the interfacial tension between the gel precursor and oil phase. As capillary number gives an estimate on the conditions for droplet pinch-off, to achieve the desired droplet size, flow rates should be arranged. In this manner, we have altered the flow rates of both oil and gel solutions depending on the gel compositions (Table 2.1).

Sample	**GelMA% (w/v)**	**HAMA% (w/v)**	**Collagen% (w/v)**	***Q_c (μL/h)**	***Q_d (μL/h)**
GelMA (10)	10%	–	–	600	60
GelMA:HAMA (9.25:0.75)	9.25%	0.75%	–	370	40
GelMA:HAMA (8.75:1.25)	8.75%	1.25%	–	370	40
GelMA:Collagen (8.75:1.25)	8.75%	–	1.25%	600	40
GelMA:Collagen (7.5:2.5)	7.50%	–	2.50%	600	40

Table 2.1: Table showing the composition of GelMA, HAMA, and Collagen samples along with flow rates Q_c and Q_d. *Q_c: Continuous phase (Silicon Oil) flow rate. Q_d: Dispersed phase (Gel Precursor) flow rate.

Proceeding to this, to evaluate the size distribution of the microgel droplets, coefficient of variation (CV%) was calculated for 10% GelMA as our reference sample, and it was found as 1.05% which shows a highly monodispersed droplet generation (Figure 2.2b). In addition, spherical shape and monodispersity were maintained by the microgel droplets upon polymerization as well (Figure 2.3a). upon 1 minute of in situ photopolymerization, the microgels were treated with IPA to remove the oil phase of the droplet microfluidics chip and dried over mild heat ($\tilde{4}5$°C) for few mins (Figure 2.2c). This resulted in a preserved structure of

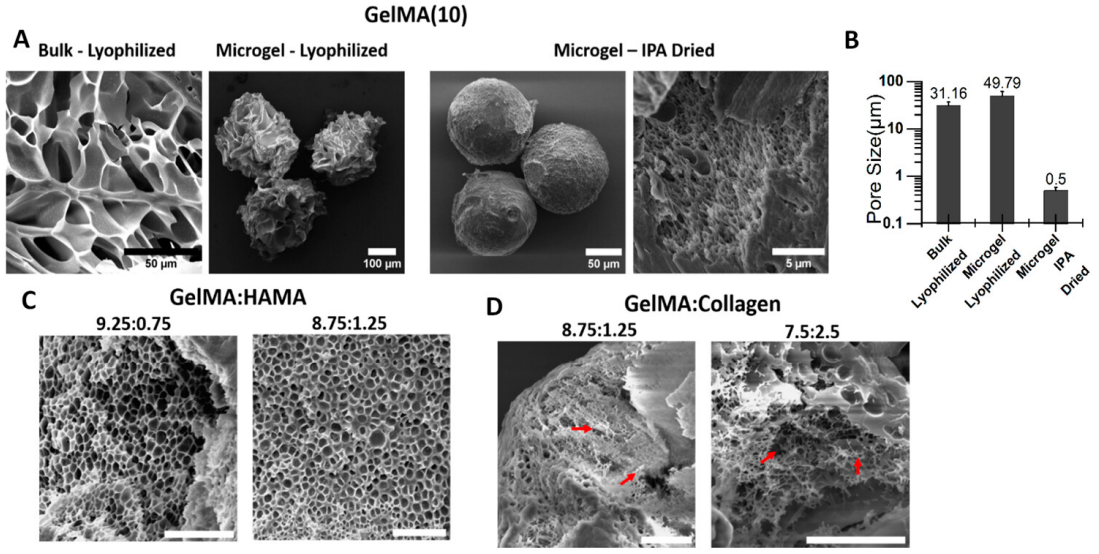

Figure 2.3: SEM images of different gel compositions. (a) Comparison of GelMA(10) in lyophilized bulk form and IPA-treated microgel form and (b) comparison between the pore sizes versus drying procedure, with the pore size on the logarithmic scale (base 10). (c) IPA-treated GelMA/HAMA hybrids revealing porous structure with differing wall thicknesses. Scale bars: μ m. (d) GelMA/collagen hybrids showing interpenetrating structure, with collagen fibrils filling the pores of GelMA indicated with red arrows. Scale bars: 5 μm.

microgels without effecting the shape as well as porosity both in bare and hybrid microgel compositions.

2.3.3 Structural Analysis of Microgels

Understanding the structure of hydrogels is of great importance since this property effects such as the nutrient transport, stiffness, water retention capacity, degradation rate and cell response to the environment among many others. In literature, morphological analysis of microgels is mainly carried out with freeze drying procedures on their bulk versions[56, 57, 58] and in rare instances on microgel versions[4]. Whilst this technique provides a comparison between different compositions of hydrogels, it fails to give an accurate reflection of the microstructural specifics of hydrogels like porosity and/or wall thickness because of possible

drying artifacts. Therefore, in the current study, we desired to investigate the inner structures of microgels as accurate as possible. This was essentially achieved with the aforementioned washing and microgel collection step. Remarkably, because of their small scale, substitution of the water within the pores with alcohol, and the subsequent drying with mild heat was probable and can be carried out with ease in a short period of time. This way, microgels revealed their inner structures unchanged without the harsh conditions of freeze-drying.

As a reference, the differences between effect of freeze drying on bulk, on microgel and IPA treated microgel were also examined using 10% GelMA samples (Figure 2.3a). Lyophilization on bulk and on microgels revealed similar porous appearance, with pore sizes being approximately 31μm and 49μm, respectively. Excitingly, the IPA treated version on the other hand, showed a full sphere from the outside and an evenly distributed circular porous structure with 0.5μm pore size on the inside (Figure 2.3b). To the best of our knowledge, this study provides for the first time a realistic image of microgel pores at microscale, without any external treatments and further manipulation in the imaging protocols.

Furthermore, the addition of hybrid components (HA and collagen) to GelMA and the alterations on the internal structure were also investigated in SEM, which was quite evident such as HAMA addition resulted in a uniform porous structure with an increase in the pore wall thicknesses and a subsequent decrease in the pore size with respect to increasing HAMA content in microgels (Figure 2.3c). Contrary to the Collagen addition, GelMA and HAMA were forming a copolymer network, therefore a change in the porosity of gels was expected. Whereas, with Collagen incorporation, the expected interpenetrating network revealed itself as a porous structure accompanied by a dense meshwork formed by Collagen fibrils (Figure 2.3d). In addition, with GelMA:Collagen (7.5:2.5) samples, meshwork was more prominent with less pores visible, and the opposite observation was valid for GelMA:Collagen (8.75:1.25) (Figure A.2). With the conditions of lyophilization, this network reveals itself as a thick-walled porous structure causing a non-informative picture[59].

2.3.4 Swelling Behavior of Microgels

The ability to understand and manipulate the swelling behaviors of microgels carries great significance since this attribute is tied to waste and nutrient transport, absorption kinetics, drug release and the dynamics of microgel volume change. Our initial approach on examining the swelling behaviors was to place the dry microgels onto a glass slide and observe the volume change with the addition of a drop of buffer on top. This method failed due to a couple of reasons. Firstly, microgels were either sticking to the surface, which meant swelling did not occur through this side of the gel or were floating to the buffer-air interface which caused manual intervention to force the gel into the buffer droplet. Secondly, following each gel to examine their swelling behavior was laborious due to the mobility of gels that came with their non-constraint environment.

Hence, we switched to a custom-made platform composed of a reservoir with several wells that accommodate individual microgels (Figure 2.4a,b). This platform enabled us to swell separate microgels in a stationary manner and observe them dynamically. Furthermore, microgels were able to swell from all sides simultaneously. Following this procedure, swelling results were quantified by observing the volume changes. As predicted, the addition of hybrid components to GelMA revealed itself in swelling behaviors and confirmed the ability to control the swelling pattern without altering the total gel concentration in the hydrogels.

Adding Collagen at varying percentages the swelling pattern of microgel pursued an increasing trend in the volume fold swelling at first, from 676% to 839% when compared the reference GelMA(10) and GelMA:Collagen(8.75:1.25) hybrids; however, as the concentration of Collagen was increased to 2.5%, swelling of microgels got suppressed to 613%. It is defined that degree of swelling of the hydrogels is interrelated with the extent of crosslinking, which eventually affects the mechanical strength of hydrogels. Similarly, the extent of hydrophilicity of individual polymer also plays a significant role in the overall behavior of the hydrogels[60]. In agreement with this understanding, as the concentration of the polymer (collagen) increased from 1.25% to 2.5% (Figure 2.4c) with the reference

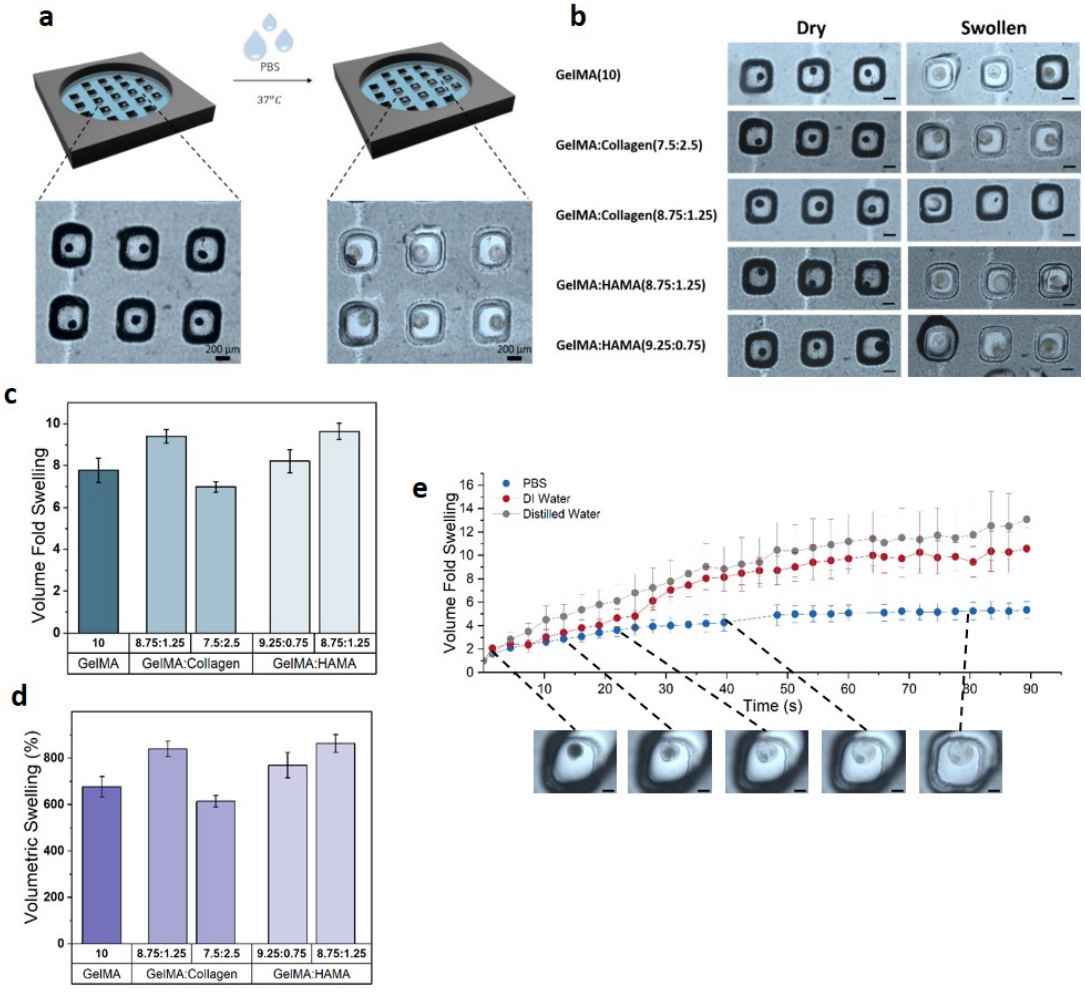

Figure 2.4: Examination of the swelling behaviour of microgels. (a) A custom-made platform was utilized for swelling characterizations. (b) Each dry gel was placed into respective wells and their swelling behaviour was observed with the addition of PBS. (c, d) Swelling was quantified through calculating Volume Fold Swelling and Volumetric Swelling (%). (e) The platform also enables the examination of the dynamic volume change in real-time. Swelling of GelMA(10) microgels in PBS, DI water and distilled water were used to demonstrate this ability with images belonging to PBS swelling. Scale bars: 100 μm.

GelMA(10) hydrogel, the degree of swelling dropped from 839% to 613%.

Conversely, for HAMA hybrid compositions, increasing the amount of HAMA within microgels resulted in increased volume fold swelling due to strong hydrophilic nature of HA. It is also stated in the literature that high ratios of HAMA in hybrid gels increases the swelling degree of the product[19], which is supported with the results obtained herein (Figure 2.4 c,d). Several physiochemical aspects of HA are advantageous for such properties. For instance, HA is highly hydrophilic and in biomedical applications; this high-water absorption capability enables the transport of metabolites and nutrients and conserve the resiliency of hydrogels. It also offers controlled biodegradability, biocompatible polymerization chemistry, and versatile modification strategies (e.g., multiple different reaction sites), thus a good choice in several biomedical applications.

The analysis of dynamic behavior of microgels is important in understanding their absorption characteristics, and we were able to examine the swelling of GelMA(10) microgels in real-time as they were being swollen within PBS. According to the observations, fast swelling rate was measured in the initial few seconds, followed by a steady volume increase in the proceeding time period, reaching to full size after about 60 seconds.

The swelling behavior in general depends on the physicochemical properties of the gels including their hydrophilicity, surface charge and ionic strength along with some environmental factors such as temperature and pH of the surrounding medium. Therefore, for various biomedical applications in drug delivery and tissue engineering, understanding the swelling kinetics in various conditions is preferred. To this end, we also conducted the dynamic observation of GelMA(10) swelling in distilled water as well as deionized (DI) water. The results depicted a clear difference in swelling patterns of gels between these buffers, with an increase in solvent absorption and thereby swelling behavior in distilled and DI water as compared to PBS (Figure 2.4e). The data, thus, supports the previous findings on understanding the swelling behavior of GelMA in different buffers[61].

2.3.5 Enzymatic Degradation of Microgels

Examination of enzyme specific degradation is important to estimate how the microgel would behave in the specified environment. For many tissue engineering applications, the environment in question implies scarred tissues that require regeneration. Such an application requires the accurate match between the degradation rate of the gel and the formation rate of the new tissue. Similarly, in 3D cell culture applications, scaffold should remain intact until cell aggregates form and create their own ECM. On the contrary, drug release applications require the comprehensive understanding of degradation times and degradation profiles to manipulate the release rates. Such specific applications, by this means, require the thorough understanding of how microgels behave in the presence of enzymes.

With the purpose of utilizing the microwell-platform for such observations, it enabled us to examine the degradation profiles of the hybrid microgels in real time in the presence of substrate specific enzymes, i.e., collagenase and hyaluronidase (Figure 2.5a). As GelMA and Collagen possess Matrix metalloproteinases (MMPs) sequences that can be cleaved by collagenases, and GelMA was the main polymer of our microgels, we started the investigation of degradations with Collagenase. It has been recognized that collagenase is a highly specific proteinase enzyme for both native as well as denatured collagen[62]. Therefore, it transmits higher substrate specificity, and targets only collagen and gelatin among many proteins [63]. Consequently, it is considered that the collagenase specificity would be related directly with the characteristic structure of collagen.

Upon investigation of the enzymatic degradation of various hybrid microgels synthesized in this study, using collagenase at first, GelMA(10), GelMA:Collagen(8.75:1.25) and GelMA:Collagen(7.5:2.5) microgels gave almost similar degradation times; where GelMA(10) degraded completely in 51 $\pm$2 minutes, GelMA:Collagen(8.75:1.25) in 57 $\pm$ 1 minutes and GelMA:Collagen(7.5:2.5) in 64 $\pm$2 minutes (Figure 2.5b). This degradation profile shows that degradation time increases with the increasing Collagen content which can be justified with the mode of action of collagenase and how this enzyme works on Gelatin and

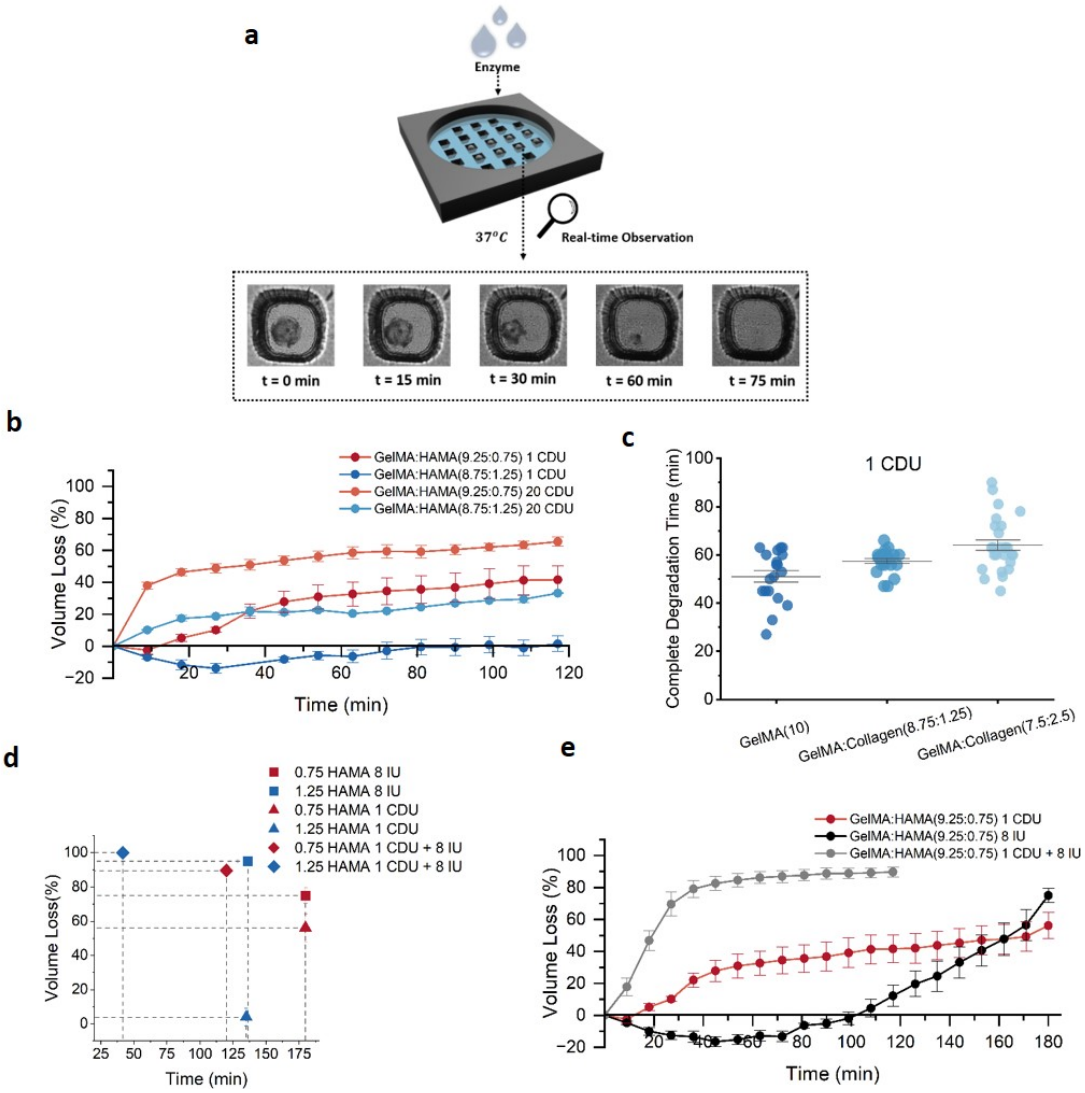

Figure 2.5: Degradation behavior of hybrid microgels in the presence of enzymes. (a) Observations were done on the microwell platform in real time. (b) Bare GelMA and hybrid collagen samples showed complete degradation in 1 CDU collagenase. (c) HAMA samples showed lower and incomplete degradations even though the collagenase concentration was enhanced by a drastic increment of 20-fold. (d and e) Furthermore, HAMA samples exhibited different degradation profiles in the presence of hyaluronidase and the combination of collagenase and hyaluronidase.

Collagen. With Collagen, Collagenase initially opens the triple helix structure of collagen fibrils, then moves on to cleaving peptide bonds[64]. In GelMA on the other hand, Collagenase directly starts cleaving the peptide bonds. Hence, it can be expected to have a slightly slower degradation pattern for Collagen-GelMA hybrid microgels as compared to GelMA alone. Remarkably, our results are aligned with the previous study reflecting the similar degradation profiles of GelMA:Collagen hybrid microgels, where increasing the concentration of collagen in the hybrids increases the overall degradation time[65].

Likewise, while monitoring the degradation data of HAMA hybrids, even though HAMA content was very low compared to GelMA, their degradation profiles showed the overpowering effect of HAMA on the microgel integrity by not giving complete degradation in the presence of collagenase. This finding of such property of HAMA, HAMA contents in general, was kept lower in the resulting hybrid microgels [66, 19].

Interestingly, by the real-time observations, one new revelation in our study has been captured that the behavior of different HAMA-GelMA hybrids in the presence of Collagenase (Figure 2.5c). As the HAMA content increased from 0.75% to 1.25%, degradation of the microgel decreased significantly. Moreover, hybrid microgels of GelMA-HAMA composition have been displayed to retain exceptional structural as well as physico-chemical properties. It has been witnessed that out of GelMA-HAMA hybrids, an increment in the HAMA polymer concentration enriches the stiffness of hydrogel, which in turn impacts the degradation behavior along with other physical parameters of the gel. However, this degradation alters with respect to the availability of the type of enzyme. Within this regard, GelMA:HAMA (8.75:1.25) showed an initial increase in the volume, followed by a slow degradation profile with 1.5% volume loss in 117 minutes, however, this volume loss was more ($\tilde{4}1\%$) for low HAMA percentage (0.75). To understand whether the collagenase amount would affect this behavior or not, a dramatic increase in the collagenase concentration, i.e., 20 CDU was subjected to the similar hybrid compositions. Interestingly, with this increment, a significant difference in the degradation pattern was monitored with respect to volume loss of the hybrids. For instance, volume loss of GelMA:HAMA (9.25:0.75) increased

to 65% from 41% in the similar time (117 minutes), while the volume loss of GelMA:HAMA (8.75:1.25) increased to 33% from 1.5%, along with no initial volume gain. The possible explanation to this difference in the degradation profile can be the availability of more than enough amount of enzyme for its substrate to produce its effect. Such as, 1 CDU was sufficient to digest the amount of GelMA in the hybrid with a slow progression of time, however, increasing the amount of enzyme (¿10 folds) for the similar composition resulted in higher digestion rate because of the availability of ample amount of enzyme to digest the same ratio of substrate, hence producing higher degradation and volume loss profile at the same time, i.e., 117 minutes. Moreover, suppression of initial volume gain can be justified with a fact that due to availability of higher enzyme content, the degradation specificity masked the effect of HAMA in this solution, thus, showing more linear degradation profile.

To further discuss and understand with our findings, a complete degradation pattern of HAMA hybrids (similar to Collagen) was also analyzed. For this, we examined the degradation of different GelMA-HAMA hybrids in the presence of a more specific enzyme for hyaluronic acid, i.e., Hyaluronidase. Excitingly, the results were different in comparison to the collagenase's effect, where increasing HAMA content resulted in much faster degradation (Figure 5d), with almost complete degradation of GelMA: HAMA (8.75:1.25) in 135 minutes, while GelMA:HAMA (9.25:0.75) lost 75% of its volume in 180 minutes. This is attributed to that due to the increase of hyaluronidase's substrate.

To shed light on the degradation behavior of GelMA-HAMA hybrid microgels, we also conducted degradation assay with combination of these enzymes (hyaluronidase and collagenase) to observe the effect of dual enzymes on the hybrid microgels. The results revealed that GelMA:HAMA (8.75:1.25) degraded much faster showing 100% degradation in only 40 minutes whereas, GelMA:HAMA (9.25:0.75) degraded 90% in two hours. The results were quite distinguishable with the degradation profile of these hybrids in the presence of single enzyme, hence, proving the enzyme-substrate specificity and relation strongly (Figure 2.5e). Likewise, if the degradation of GelMA:HAMA hybrid were to be examined with comparative representation of these enzymes (i.e. Collagenase or

Hyaluronidase) (Figure 2.5e), it can be comprehended that these enzymes gave different degradation profiles for the similar composition of hybrids (9.25:0.75), where a rapid volume loss occurred in the initial 45 minutes with collagenase, while volume gain was observed with hyaluronidase. However, at the end of a 180-minute period, hyaluronidase caused more degradation than collagenase, correlating with our previous findings as discussed above. Combination of these enzymes on the other hand, demonstrated a much rapid degradation profile, causing 80% volume loss in the first 1 hour, reaching to 90% in the remaining 1 hour with a slow trend.

The mentioned initial volume gain can be due to the enzyme-substrate activity and an initial relaxation in the polymer. It can be seen that the volume gain was observed in GelMA:HAMA (9.25:0.75) in the presence of hyaluronidase and GelMA:HAMA (8.75:1.25) in the presence of collagenase. As previous results have showed, in GelMA:HAMA hybrids, HAMA is the dominant component. Because of this, GelMA:HAMA (8.75:1.25) sample showed a slow degradation profile and very little volume loss with collagenase. As collagenase amount was increased to 20 CDU, however, due to an increase in enzymatic attack on GelMA, degradation was swift and volume loss was increased. Similarly in GelMA:HAMA (9.25:0.75), whilst HAMA's presence was still dominant on GelMA it was not as much compared to GelMA:HAMA (8.75:1.25). This resulted in GelMA:HAMA (9.25:0.75) showing faster response to collagenase due to increased enzyme-substrate interactions. However, hyaluronidase still caused higher volume loss at the end, with a slow degradation profile. These slow degradation profiles revealed the initial volume increases, which may be due to the initial relaxation in the polymer and the subsequent revelation of hydrophilic groups that were suppressed by the dense connections in the network initially. However, as time passed, the polymer began to lose its structural integrity and started to collapse on itself leaving the non-enzyme specific polymer behind, hence the volume losses[67].

2.4 Conclusion

In this study, we propose physical characterization assays curated for hybrid-microgels to examine their inner structures and understand their swelling and degradation behaviors in real-time under different conditions. To reveal new behaviours of individual hybrid microgels at single microgel level, we used GelMA polymer complemented with Collagen and HAMA. As microgels' physical behaviors are affected by their size and shape, we utilized a droplet microfluidic chip to achieve monodispersed spherical microgel production in a high throughput manner. Upon production, we washed and collected individual microgels to substitute the commonly used lyophilization process, which revealed a more accurate picture of their inner structures and morphology. To examine individual microgels' swelling and degradation behaviors, we fabricated a customized micro-well platform to accommodate one microgel in each well stationary, while allowing access to the solution in a 3-dimensional manner. Experiments carried out in this custom-made platform revealed previously unseen results that confirmed the necessity of new assays for investigating microgel behaviors. Excitingly, this platform offered, for the first time, to carry out real-time examinations of swelling and degradation behavior of individual hybrid-microgels in an agreeable 3D version, with real-time statistics for each combination of gel materials. We believe that the proposed assays will help accelerate microgel utilization in biomedical sciences by comprehensively understanding their physical characteristics.

Chapter 3

Capturing the Changing Scaffold Properties of HAMA/GelMA Microgels During Enzymatic Degradation

3.1 Introduction

Profiling the temporal changes a scaffold undergoes due to cellular activity is essential for optimizing scaffold design and utilization in tissue engineering. Understanding how scaffold properties evolve during degradation allows for the creation of dynamic environments that better mimic the natural tissue healing process. For instance, depending on the mode of degradation, a scaffold's volume may decrease while stiffness remains constant, or stiffness and mass may decline while volume stays the same. In microgels, where directly capturing mass changes is challenging due to their small size, monitoring stiffness variations can reveal correlations between volume and mass, indirectly indicating changes in polymer structure and porosity. Such holistic evaluation becomes especially important in designing scaffolds with temporally controlled degradation rates. By profiling these temporal changes in mechanical properties, porosity, and biochemical signals, researchers can design scaffolds that deliver targeted cues at optimal times, improving regenerative outcomes. This approach also extends to applications such as drug delivery, where scaffold degradation can be tuned for controlled and sustained release of therapeutics. Ultimately, leveraging the temporal evolution of scaffold properties allows for tissue engineering strategies that align scaffold behavior with the dynamic needs of regenerating tissues, leading to more predictable and successful clinical outcomes.

In this chapter, we examined the physical and mechanical changes microgels produced with droplet microfluidics go under during enzymatic degradation. We chose to examine GelMA and HAMA copolymer networks having different ratios. GelMA, a photocrosslinkable gelatin derivative, is widely utilized as a scaffold for tissue engineering applications because of its similarity to collagen, having cell attachment motifs, and being biodegradable.[68] Similarly, HAMA is a hyaluronic acid derivative that is also photocrosslinkable with motifs guiding immune response, cell differentiation, and proliferation. [69] Crosslinked together, they create a scaffold that is biocompatible, mechanically tunable, and bioactive, with a wide range of versatility in applications. [24] Produced with droplet microfluidics and crosslinked in situ, uniform copolymer microgels are fabricated from these

materials. These microgels are degraded with collagenase and hyaluronidase, and changes in their volume, topology, stiffness, and compound release are followed.

3.2 Materials and Methods

3.2.1 Gelatin Methacryloyl(GelMA) and Hyaluronic Acid Methacrylate(HAMA) Synthesis

GelMA and HAMA are synthesized separately by modifying Gelatin and Hyaluronic Acid with methacrylate according to previous protocols with slight alterations.[19]GelMA synthesis starts by dissolving 10% (w/v) gelatin in phosphate-buffered saline (PBS) at 60 °C degrees under continuous stirring. Once complete dissolution was achieved, 5% Methacrylic Anhydrate (MA; v/v) was added dropwise over 2 h. The solution is left to react for 3 h at 50 °C, followed by quenching with an equal amount of warm PBS. To clear the solution from byproducts and unreacted MA, dialysis with 12-14 kDa cutoff is performed at 40 °C for 5-7 days. The final product was kept at -80 °C overnight and then lyophilized for a week.

For the HAMA synthesis, 1%HA (w/v) is dissolved in PBS with slow additions and continuous stirring over 24 h at room temperature. Following complete dissolution, 5% MA (v/v) is added dropwise over a few hours by keeping the pH between 7 and 10 with the continuous addition of 5 M NaOH at 4 C. After 3 h of reaction, the solution is diluted with an equal volume of PBS and dialyzed against distilled water at 4 **°C** in a 12-14 kDa dialysis membrane for a week. The solution is frozen at -80 °C overnight and lyophilized for 3-5 days.

3.2.2 Degree of Methacrylation (DM) of Gelatin and HA

GelMA and HAMA's degree of methacrylations were quantified with ^{1}H NMR. For GelMA, 20 mg of GelMA and bare gelatin (control) were dissolved in 1 mL of D_2O, and stored in 37 °C until measurements. In the case of HAMA, 5 mg of HAMA and HA (control) were dissolved in 1 mL of D_2O at room temperature.

The spectras were evaluated as follows to calculate DMs. For GelMA, the

spectras of gelatin and GelMA were normalized with respect to the phenylalanine signal located at 6.9-7.5 ppm, which is expected to depend only on the gelatin concentration and not be affected by methacrylation. Then, the area under the lysine methylene peaks at 2.7 – 2.9 ppm was calculated by integration. As gelatin is methacrylated, it is expected to observe a decrease at the lysine methylene peaks and an increase at the peaks at 5.2-5.6 and 1.9 ppm, which belong to the formed methacryloyl groups. The DM is calculated using the following equation:

$$\mathrm{DM}_{\mathrm{GelMA}} = \left(1 - \frac{A(\text{Lysine Methylene of GelMA})}{A(\text{Lysine Methylene of Gelatin})}\right) \times 100$$

For determining the DM of HAMA, the peak at 1.9 ppm in HA which belongs to methyl protons gets altered upon methacrylation, accompanied by the new peak formations at 1.5-2.0 ppm in HAMA spectra. Furthermore, the peaks at 1.8 ppm and 5.6-6.1 ppm that belongs to MA methyl protons and methacrylate vinyl groups respectively confirms the substitution. Following equation is used for DM calculation:

$$\mathrm{DM}_{\mathrm{HAMA}} = \left(1 - \frac{A(\text{HA Methyl proton peak (1.9 ppm)})}{A(\text{MA Methyl proton peaks (5.6-6.1 ppm)})}\right) \times 100$$

3.2.3 Hydrogel Precursor Preparation

Throughout the experiments, all hydrogel precursors were prepared to have a final 10% (w/v) gel content in the working solutions. Therefore, bare GelMA hydrogel is prepared by dissolving 10% lyophilized GelMA in PBS at 37 °C.

HAMA and GelMA hybrid networks were prepared by initially dissolving HAMA in PBS under continuous stirring at room temperature. Following, the solution temperature was raised to 37 **°C**, and GelMA was added and mixed until complete dissolution. Following the same protocol, 3 different GelMA: HAMA compositions were prepared: GelMA:HAMA(9.25%:0.75%), GelMA:HAMA(9%:1%), and GelMA:HAMA(8.75%:1.25%).

Finally, to any solution mentioned above, 0.5%(w/v) lithium phenyl-2,4,5-trimethylbenzoylphosphinate (LAP) was mixed in as the photoinitiator.

3.2.4 Chip Fabrication

The droplet microfluidic chip consists of a PDMS layer with channels and a glass slide as a substrate. For the fabrication of PDMS mold soft lithography techniques were utilized similar to our previous works. [49]Briefly, SU-8 masters were fabricated onto silicon wafers. The PDMS prepolymer was prepared out of 10:1 ratio of base to curing agent, degassed in a vacuum chamber, and molded against the master, followed by curing at 95 °C for 2 h. After removing the mold from master, 1.5mm punch holes were made using biopsy punches at the inlets and outlet. The mold was then oxygen plasma treated at 100 W and 400 mTorr for 30 seconds and bonded to the glass slide.

3.2.5 Microgel Production and Collection

Microgels were produced with a droplet microfluidic chip with three main regions: a droplet formation part, a serpentine section, and an outlet. The droplet generation comprises a flow-focusing design connected to two inlets for the hydrogel precursor and oil entries. A serpentine section follows the droplet production. After the serpentine, another inlet for oil is utilized to increase the distance between droplets, which the outlet follows. The outlet was a hole punched on the side of the chip connected to a tubing for horizontal flow. The microgels are then cured in this tubing, 3-5 cm away from the chip. Silicon oil (50 cSt) with 2% surfactant was used as the continuous phase in all cases. The chip was placed onto a microscope (Zeiss, Axio Observer 7 inverted microscope) equipped with an incubation system to maintain the incubation chamber at 37 °C. Syringe pumps were used to drive the gel and oil flows, and droplet formation was observed under the microscope. Once the droplet production was stable, the microgels were allowed to polymerize (405 nm, 350 mW/cm2).

To confirm the monodispersity of droplets, the coefficient of variance (CV) was calculated as follows:

$$\mathrm{CV}(\%) = \frac{\sigma_{\mathrm{microgel}}}{\mu_{\mathrm{microgel}}} \times 100$$

$$\sigma_{\mathrm{microgel}} = \text{Standard Deviation of the distribution}$$

$$\mu_{\mathrm{microgel}} = \text{Mean of the distribution}$$

3.2.6 Post-Processing of Microgels

After collecting microgels with oil from the chip into the Eppendorf, the oil is removed to a large extent with centrifugation. 5%(v/v) Span80 in PBS at 37 °C is added on top of the settled microgels and vortexed to dissolve unpolymerized gels, if there were any, in addition to break the interface between microgels and oil phase. This step is repeated three times with centrifugation. The washing is finished off with Isopropyl Alcohol (IPA) cleaning to clean the microgels from oil completely and eventually dry them. IPA is added to the microgels, vortexed, and centrifuged three times. Microgels in IPA were strained through a cell strainer and placed onto the hot plate at 35 °C to dry overnight. Alternatively, they were aliquoted into 0.5 mL Eppendorfs in certain numbers and placed onto the hot plate at 35 °C to dry overnight. Dried products were kept in the fridge until further use.

3.2.7 Biodegradation of Microgels

Biodegradation of microgels was carried out using collagenase and hyaluronidase. A predetermined number of microgels were first swelled in an Eppendorf with 200 μl PBS and transferred to the well of a 96-well plate. Within seconds, microgels settle to the bottom, and 150 μl of PBS is drawn with a micropipette from the top of the well slowly so as not to disturb the microgels. 150 μl of enzyme solution is prepared to have a final concentration when added to the well, where the total

will be 200 μl. The enzyme concentration used for the experiments was 0.125 CDU 1 IU and was prepared freshly from the stock solutions of 0.0625CDU/μl collagenase and 0.1IU/μl. The prepared enzyme solution is added to the 50 μl of microgel plus PBS, followed by the start of the experiment at the microscope with the chamber temperature at 37 °C.

Upon image acquisition, volume loss and complete degradation times were quantified where appropriate. If the microgels degraded through surface erosion and kept a spherical shape, volume left was calculated as follows:

$$\text{Volume Left } (\%) = \frac{V_t}{V_0} \times 100$$

V_0 corresponds to swollen microgel volume at time 0, while V_t is the volume at later stages.

In the case of bulk degradation, the complete degradation time was determined by analyzing the obtained images.

3.2.8 Porosity and Topology Characterizations

To examine the porosity and topology during degradation or not, light microscopy and SEM are utilized. The dried versions were examined under SEM. Microgels were cut in half using a needle to access the porous inner structures. Cut versions were placed on silicon wafers and were sputter-coated with an ultrathin layer of gold/palladium before imaging with SEM.

3.2.9 Capillary Micromechanics for Stiffness Measurement

The capillary micromechanics method was employed to quantify the compressive modulus of the microgels during biodegradation.[70, 71]The measurement setup includes a tapered glass capillary (tapering angle a = 0.087 radians) with the tip

opening to a reservoir on a glass slide and back connected to the tubing. At the start of the experiment, 0.1%BSA in PBS (w/v) is flushed through the capillary to minimize the friction between microgels and the inner surface of the capillary. Then, a dilute suspension of microgels in PBS is driven by the hydrostatic pressure difference(p) applied to a high-precision pressure pump (Fluigent). Due to the capillary tip having a smaller diameter than the microgels, one microgel reaches the tip and blocks the flow further. At that point, the whole pressure difference falls onto the microgel, resulting in the microgel deforming both in shape and volume. When the particle no longer moves or deforms at equilibrium, an image is acquired. The pressure difference is increased in increments until the microgel reaches the very tip, and the images are taken at every increment. This process is carried out for different compositions of microgels degraded in 0.125 CDU plus 1 IU enzyme concentration and on samples taken at hourly time points over the span of 6 hours. In detail, 100 to 150 microgels were degraded but for a predetermined time. At each time point, the microgels were removed from the 96-well plate, washed with PBS, and dispensed into the pressure pump's vial.

The compressive modulus (K) is calculated using the values of the contact length between the deformed microgel and the capillary wall (L_{band}) and the radius of the middle point of the deformed microgel (R_{band}) obtained from the images using image J with the following equations:

$$K = \frac{\frac{1}{3}\left(p_{\text{wall}} + p\right)}{2\varepsilon_r + \varepsilon_z}$$

$$p_{\text{wall}} = \frac{p}{\sin(a)} \cdot \frac{R_{\text{band}}}{2L_{\text{band}}}$$

Where p_{wall} is the wall pressure and ε_{r} and $\varepsilon_{\text{z}}$are strains in the r and z directions(cylindrical coordinates, z-direction is the central axis of the capillary).

The compressive modulus is a measure of the material's resistance to volume change where the stress comes from the hydrostatic pressure $\sigma_{\text{compr}} = \frac{2p_{\text{wall}}+p}{3}$ and the strain is volumetric strain $\frac{\Delta V}{V} \approx 2\varepsilon_{\text{r}} + \varepsilon_{\text{z}}$. The modulus is determined from the slope of σ_{compr} as a function of $\frac{\Delta V}{V}$.

For each time point, the average of the compressive modulus of 10 microgels

was taken.

3.2.10 Model Drug Release

For the drug release studies, the microgels are loaded with Rhodamine B, Fluorescein, and Congo Red. To load the microgels with model drugs, 100 to 120 microgels were incubated overnight in an Eppendorf with 0.1mg/mL for Rhodamine B and Congo Red, and 0.01mg/mL for Fluorescein in PBS buffer solution at 37 °C. Following, they were cleaned with PBS in a cell strainer to remove excess and transferred to a new Eppendorf. To start the experiment, 0.125 CDU plus 1 IU enzyme solution (200 μl) was added on top, and incubation was continued at 37 °C. To estimate the release, 100 μl of supernatant was withdrawn, and fresh enzyme solution of the same amount was added hourly for 6 hours. Together with the remaining after the 6th hour, samples of each hour's fluorescence were measured with a microplate reader. (Excitation and emission for each model drug were as follows: 544-590nm for Rhodamine B, 485-538 nm for Fluorescein, and 584-612nm for Congo Red) An average of three experiments was taken for quantification, and percentage release was calculated from the fluorescence values (A.U.). The release data is then fitted using Korsmeyer-Peppas equation,

$$\frac{M_t}{M_\infty} = kt^n$$

Where $\frac{M_t}{M_\infty}$ is the fraction released at time t, k is the kinetic constant, and n is an indicator of transport mechanism.

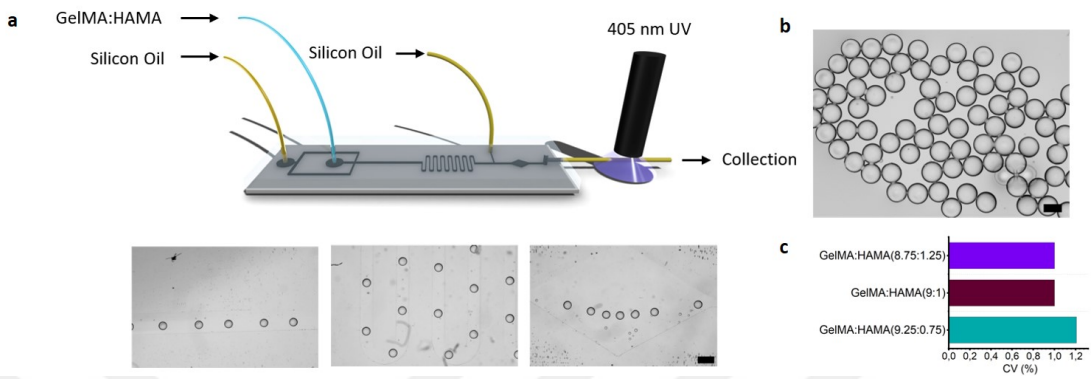

Figure 3.1: Droplet microfluidic production. (a) Microfluidic chip and microscopy images depicting different parts of the chip. Scale bar 500μm. (b) Microgels right after collection. Scale bar 200μm. (c) CV(%) calculation for each composition

3.3 Results

3.3.1 Microgel Production

GelMA and HAMA were synthesized by methacrylating Gelatin and Hyaluronic Acid. The degree of methacrylation, an indicator of the polymerization strength, is found to be 77% for GelMA and 97% for HAMA. The two solutions were mixed in different percentages to achieve a final of 10% polymers in the working solution.

To produce uniform microgels, droplet microfluidics is utilized. Droplets produced from GelMA and HAMA compositions travel downstream of the chip and get further separated from each other with a secondary oil flow (Figure 3.1a). The flow rates are arranged to adapt to the changing viscosity of the compositions and to keep the droplet diameter stable at 220-250 μm. Utilizing a UV source (405 nm), droplets are polymerized in the tubing outside the chip. To check the uniformity of microgels, CV(%) is calculated for each composition, and monodispersity is confirmed with CV values at 1% to 1.2% (Figure 3.1b,c)

3.3.2 Volumetric Change of Microgels During Enzymatic Degradation

Understanding the temporal volume changes of microgels is key for optimizing their use in drug delivery, cell carriers, and tissue scaffolds. Volume changes affect drug diffusion rates and release kinetics, which are crucial for controlled delivery. For tissue scaffolds, controlled degradation and volumetric adjustments promote better integration and tissue remodeling.

To this end, GelMA hybrids are first swelled in PBS and then degraded in Collagenase and Hyaluronidase. The degradation assays involve degrading 100 to 120 microgels of each composition in 0.125 CDU 1 IU/200 μL to compare the degradation mode and speed of each hybrid. Additionally, we vary the number of microgels to assess how the quantity influences the degradation process, and we examine how different enzyme concentrations affect degradation. These assays provide a comprehensive understanding of how the compositions behave when injected into tissues with varying enzyme compositions and cavity volumes.

Examination of the degradation of 100 to 120 GelMA: HAMA hybrids under 0.125 CDU 1 IU collagenase and hyaluronidase mixture showed that as the HAMA concentration increases, the degradation time increases (Figure 3.2a). The volume changes are examined over the course of 14 hours, and GelMA:HAMA(9.25:0.75) degraded fully at the 8^{th} hour, while GelMA: HAMA(9:1) and GelMA: HAMA(8.75:1.25) had volume remaining at around 40% and 80% respectively. Increasing the enzyme amount 8 folds to 1 CDU 8 IU (Figure 3.2b), the volume changes and degradation profiles followed a similar trend with GelMA:HAMA(9.25:0.75) GelMA: HAMA(9:1) degrading fully at around 1.5 and 3^{rd} hours, and GelMA:HAMA(8.75:1.25) having around 20% of its volume left at the end of 14^{th} hour. The pattern changed when the enzyme concentration was kept at 0.125CDU 1IU, but the number of microgels was doubled to 200-250 (Figure 3.2c). In that scenario none of the compositions fully degraded in the scope of 14 hours. GelMA:HAMA(9.25:0.75) along with GelMA: HAMA(8.75:1.25) losing 40% of their initial volumes, while GelMA: HAMA(9:1)

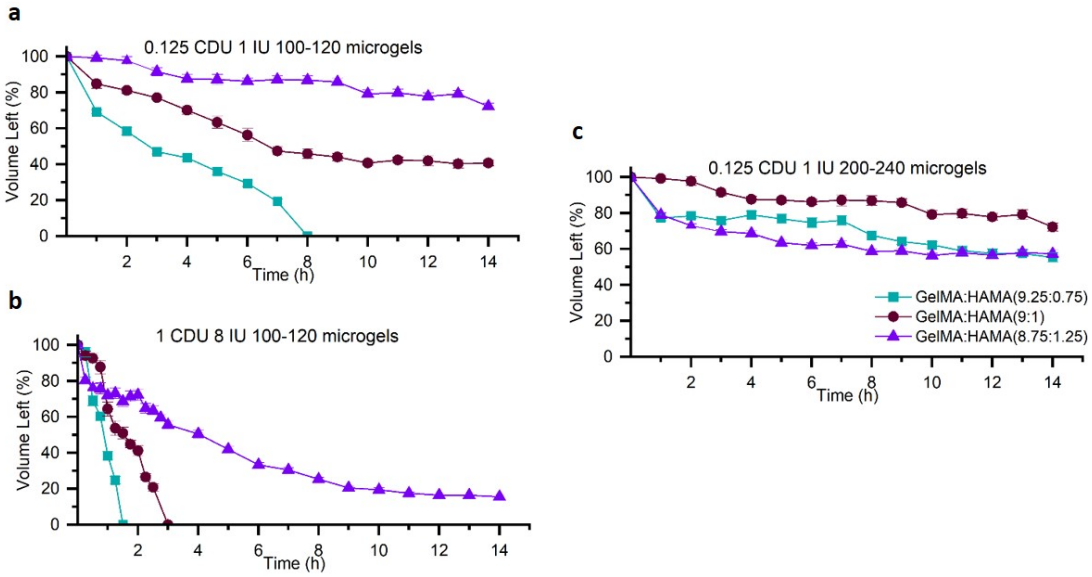

Figure 3.2: Degradation of GelMA:HAMA microgels under different conditions. (A) 0.125 CDU 1 IU with 100-120 microgels. (B) 1 CDU 8 IU with 100-120 microgels. (C) 0.125 CDU 1 IU with 200-240 microgels.

losing 20% of its volume.

3.3.3 Changes in the Surface Topology

Surface topographical features such as ridges, steps, and grooves play a pivotal role in guiding cytoskeletal assembly and cell orientation. Textured surfaces, including nodes, pores, and random patterns, significantly influence cell morphology, activities, and the production of autocrine and paracrine regulatory factors compared to smooth surfaces. The topology of microgels is crucial for cell adhesion, proliferation, and differentiation. During biodegradation, changes in surface topology can alter cell interactions with microgels, thereby affecting tissue regeneration outcomes.

Before degradation, the microgels were examined under SEM to evaluate their inner structures. GelMA:HAMA(9.25:0.75) had pores uniformly distributed from the perimeter towards the center with a pore size of 330±63 nm and

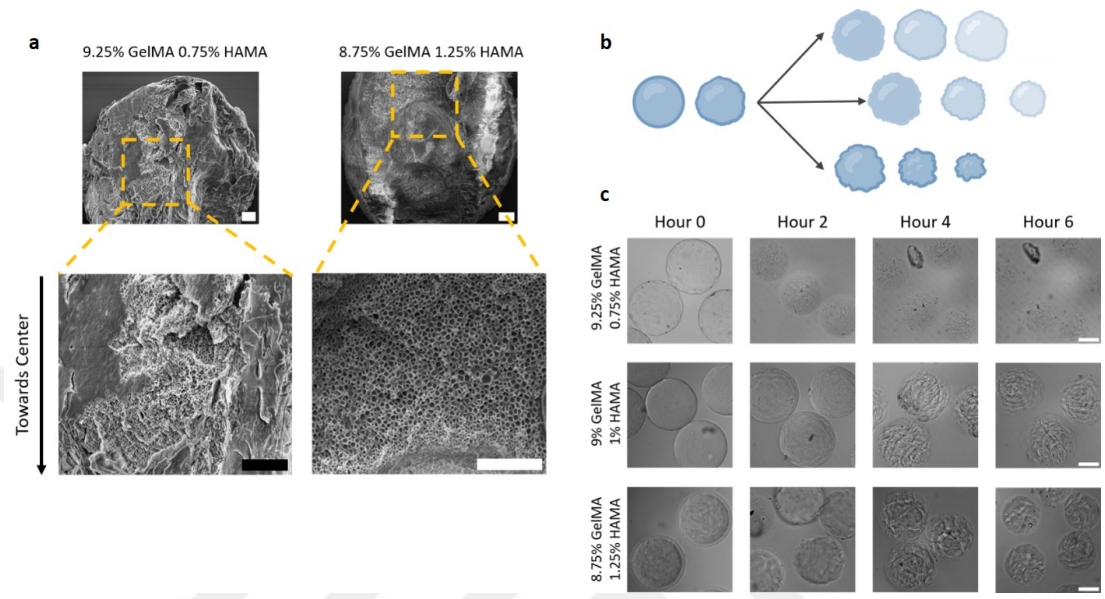

Figure 3.3: Morphology examination of microgels. (A) Inner structures of GelMA:HAMA(9.25:0.75) and GelMA:HAMA(8.75:1.25). Scale bars 10μm. (B) Observed degradation modes of microgels. (C) Changes in the morphology of microgels over the scope of 6 hours. Scale bars 100 μm.

GelMA:HAMA(8.75:1.25) revealed a decreasing porosity towards the center with the pore sizes dropping from 600±105 nm to 260± 68 nm.(Figure 3.3a) The microgels are degraded in 0.125 CDU 1 IU enzyme solutions under continuous observation to evaluate the morphological changes they go through. During this period, it was observed that the microgels degraded in different modes. They degrade through their surface and lose volume, degrade as bulk, and appear more transparent with time or showcase both of these qualities (Figure 3.3b). Furthermore, their surface starts off as relatively smooth but gains texture over time. Bulk degradation was more prominent in GelMA:HAMA(9.25:0.75), and surface degradation was more prominent in GelMA:HAMA(8.75:1.25). With GelMA:HAMA(9:1), neither degradation form was overpowering as the microgels both got smaller in size and became transparent simultaneously. (Figure 3.3c)

3.3.4 Temporal Profiling of Stiffness Change

In the design of biomaterial scaffolds for tissue engineering, it is essential for the mechanical properties of the material to resemble those of the tissue being replaced closely. This consideration is critical due to the interplay of cellular and macroscopic mechanisms. Cells interact with scaffolds through mechanotransduction, converting mechanical signals into biochemical responses that are fundamental for processes such as mobility, proliferation, migration, and differentiation. Additionally, scaffolds must support the load-bearing functions of the organ during rejuvenation. Post-implantation, enzymatic activity can disrupt the polymeric structure of the material, causing its mechanical properties to evolve over time and prompting cells to respond accordingly. To maintain homeostasis during tissue repair and regeneration, it is imperative to study how a scaffold's stiffness changes over time. This understanding is vital for both material design and predicting cell behavior.

To measure the stiffness of microgels, the capillary micromechanics method is utilized. It is a specialized mechanical characterization technique developed for deformable isotropic polymeric microspheres. It addresses the limitations of traditional methods that require bulk samples, involve laborious handling, or provide only localized measurements.

With the capillary micromechanics method, the stiffness change of degrading microgels is followed. Degradation conditions were 0.125 CDU 1IU for 100-120 microgels. The stiffnesses were followed hourly. Each microgel was placed inside the capillary and pushed towards the tip with increasing hydrostatic pressure difference. (Figure 3.4a) As the pressure increases, the microgels deform and elongate, with their length decreasing and width increased. These values are then utilized to draw a stress-strain graph. The onset of degradation and the first hours of it for GelMA:HAMA(9:1) and GelMA:HAMA(9.25:0.75) revealed an exponential graph known as strain stiffening, while their following hours and GelMA:HAMA(8.75:1.25) followed a linear trend (Figure 3.4b). Before degradation, the stiffness of microgels was 60 kPa, 42 kPa, and 33 kPa for

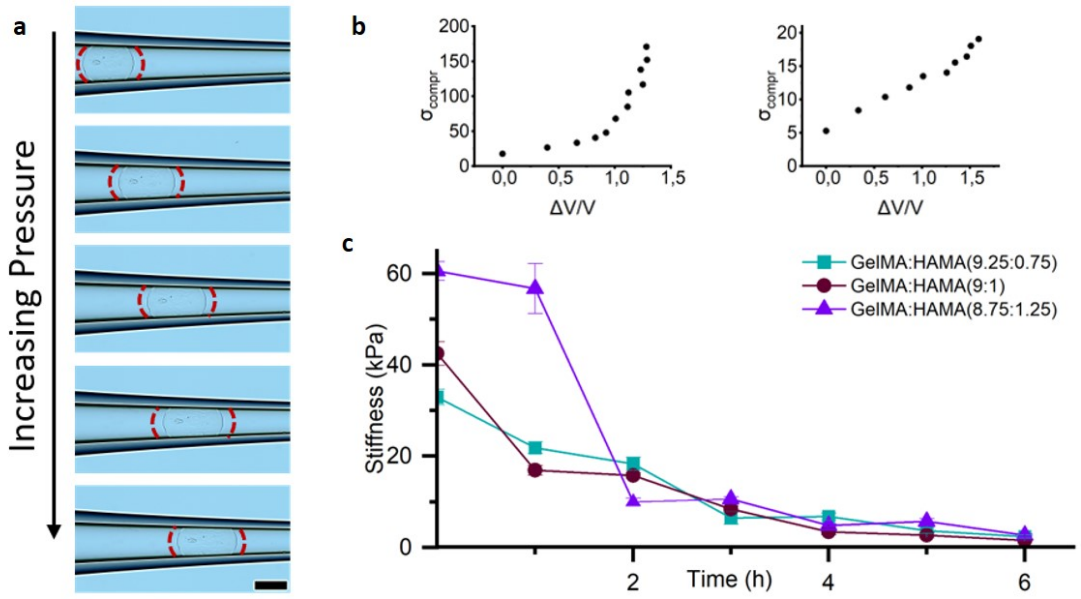

Figure 3.4: Stiffness measurement of microgels. (A) Movement of microgels towards the capillary tip with increasing pressure. Scale bar 200 μm. (B) Exponential and linear trends were observed during measurement. (C) Stiffness change of microgels with time under enzymatic degradation.

GelMA:HAMA(8.75:1.25), GelMA:HAMA(9:1), and GelMA:HAMA(9.25:0.75) respectively. In the first hour, the stiffness of GelMA:HAMA(8.75:1.25) dropped to 56 kPa, GelMA:HAMA(9:1) to 17 kPa, and GelMA:HAMA(9.25:0.75) to 21 kPa. In the second hour, GelMA:HAMA(8.75:1.25) had a stiffness of 10 kPa, GelMA:HAMA(9:1), and GelMA:HAMA(9.25:0.75) having close values of 15 kPa and 18 kPa. In the following hours, their stiffnesses changed at a slower, steady pace and reached around 2 kPa at the end of the sixth hour. (Figure 3.4c)

3.3.5 Model Drug Release During Enzymatic Degradation

Incorporating delivery systems within 3D scaffolds provides a crucial platform for achieving precise temporal and spatial control in tissue constructs. This approach enables the release of bioactive factors, offering direct instructive and regenerative signals while minimizing side effects in unintended areas. The release of

soluble factors from scaffolds can occur through various mechanisms, including diffusion, dissolution, scaffold or carrier degradation, and external stimuli. In the context of enzyme-responsive smart biomaterials, solute release is governed by both diffusion and degradation processes. Understanding the mode of degradation is essential for accurately interpreting drug release profiles and optimizing therapeutic outcomes.

To check the drug loading and release mechanisms GelMA:HAMA networks, Rhodamine B, Fluorescein, and Congo Red were selected as model drugs. Their release from GelMA:HAMA compositions during degradation with 0.125 CDU 1 IU were examined over the course of six hours. For Rhodamine B the 80 to 90% of load was released at the end of 1^{st} hour, followed by a plateau (Figure 3.5a). Fluorescein, followed a similar trend, with 75 to 80% of the load being released in the 1^{st} hour, with slight increases over time, and releasing 95 to 100% at the end of the 6^{th} hour. (Figure 3.5b) Congo Red release showed a different profile with a steady profile over 6 hours, releasing 65 to 80%. (Figure 3.5c) The data obtained was fitted with the Korsmeyer-Peppas equation to understand the release modes. The parameter n was evaluated for all cases and was below 0.1 for Rhodamine B release, below 0.2 for Fluorescein, and between 0.5 to 0.7 for Congo Red release.(Figure 3.5d) Furthermore, regardless of the model drugs, no significant difference between the release profiles of different compositions was observed.

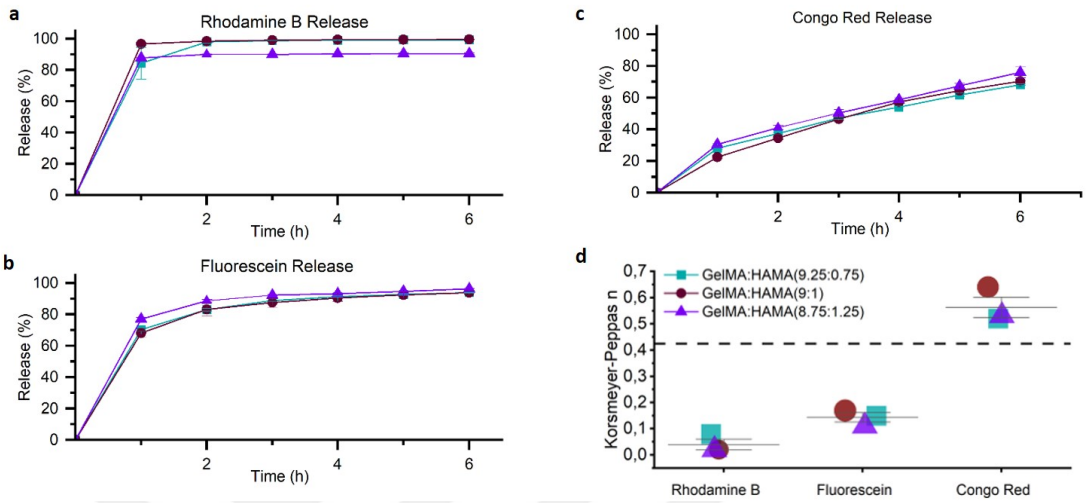

Figure 3.5: Model drug release from microgels. (A) Release of Rhodamine B. (B) Release of Fluorescein. (C) Release of Congo Red. (D) The parameter n from Korsmeyer-Peppas equation, indicating the drug release mechanism.

3.4 Discussion

Substrate mechanics and physical properties play an important role in determining the cell fate. When a scaffold is utilized for tissue engineering, it interacts with a highly dynamic environment. Through its interactions with the resident cells and soluble factors, the scaffold and environment enter into a feedback loop. This reciprocal communication constantly changes the scaffold and the cell response. Among various shapes and production techniques, microgels produced with droplet microfluidics have become quite popular in recent years. Owing to the uniformity in their shape and size, giving large enough pore sizes and being injectable, shear thinning, and self-healing without any additional chemistries, it is predictable that microgel utilization for tissue engineering will only be more important.

Additionally, with polymeric structures made up of natural or ECM-mimicking materials, such as with GelMA and HAMA, the scaffold itself, because of its inherent cell instructive sites, plays a prominent role in cell proliferation, morphology, and differentiation, in addition to their surface and mechanical properties.[72]

Their susceptibility to hydrolytic and enzymatic degradation makes their temporal profiling under these conditions important.

In this study, we investigated the changes in the volume, stiffness, morphology, and drug release behavior of three different concentrations of GelMA:HAMA microgels under enzymatic degradation of collagenase and hyaluronidase. The goal was to show that the changes in these properties should be evaluated in a holistic manner and to show that the behavior of microgels and scaffolds in a broader prospect is challenging to mimic in vitro and, hence, should be approached carefully.

As the shape and size greatly affect the solute transport, the polymer amount available to interact with cells, and enzymatic activity, our first goal was to make sure that the microgels were produced in the same size. Due to gel precursors having different GelMA:HAMA ratios, their viscosities and densities were altered, which affected the flow rates used in the droplet microfluidic chip. With small arrangements, all microgels were produced with a diameter of 230-250 μm. The monodispersity was confirmed by calculating the coefficient of variance, and the values were below 1.2%. Furthermore, microgels preserved their spherical shape upon production, dry, and swelled. (Figure A.3)

After that, their volume changes during enzymatic degradation were followed. The examined variables were GelMA:HAMA compositions, enzyme concentration, and the number of microgels. The enzyme concentration was altered to mimic different environments in the body, where the cell types and ECM change, affecting the enzyme types and their concentrations. The number of microgels was altered with respect to the applications of injectable microgels, where they are placed into cavities with varying volumes. All three parameters play a part in how the microgels degrade. Throughout the study, 0.125 CDU 1 IU collagenase hyaluronidase composition is selected to examine different properties of microgels. This value was chosen based on scanning the microgel degradation over different concentrations of collagenase and hyaluronidase as a combination or separately. (Tested concentrations are given in Table A.1) When there was only hyaluronidase, microgels showed an increase

in volume. With collagenase only, they started degrading through the surface without ever completely dissolving. When they were combined, whether hyaluronidase was overpowering or collagenase was, as the number of microgels was kept stable at 100 to 120, GelMA:HAMA(8.75:1.25) degraded slower than GelMA:HAMA(9:1), followed by GelMA:HAMA(9.25:0.75). With 0.125 CDU 1 IU, over the scope of 14 hours, the trend was the same. When the enzyme concentration was increased 8 folds, the trend remained but with faster degradation times. When the enzyme concentration was stable with an increased number of microgels, the trend changed. GelMA:HAMA(9:1) lost the least volume at the end of 14^{th} hour, GelMA:HAMA(8.75:1.25) and GelMA:HAMA(9.25:0.75) losing same amount, more than GelMA:HAMA(9:1). However, It should be noted that GelMA:HAMA(9.25:0.75) and GelMA:HAMA(9:1) kept showing downwards trends, while GelMA:HAMA(8.75:1.25) plateaued at the end of 8^{th} hour. This may indicate that if followed, in the later hours, the volume losses may change. With that, the number of microgels seems to affect the degradation trends more prominently than enzyme concentration. In our previous work, we observed that when there were 8 to 10 microgels degraded in 1 CDU 8 IU, the one degrading the most was GelMA:HAMA(8.75:1.25)[49] This is most likely due to several mechanisms such as enzyme-substrate specificity, enzyme availability, and polymer density. HAMA's degradation with hyaluronidase may be slower than GelMA's degradation with collagenase. This would explain the volume gains when there is only hyaluronidase, which was observed in our previous paper as well. With the enzyme combinations, though, the trends depend on the enzyme saturations and crosslink densities with the interplay of collagenase and hyaluronidase's degradation speeds. With 100-120 microgels, and observing the same trend with 0.125 CDU 1 IU and 1 CDU 8 IU it seems that enzyme concentration is enough, and there is no competition for their availability, but their amount speeds up or slows down the process. This means that degradation profiles only depend on the crosslink densities, which indicates that increasing the HAMA concentration creates denser networks. When the microgel number is increased, though, the trends change. This means that now there is competition for enzyme availability.

The observation of their inner structures also brings up another parameter, network heterogeneity. The observed pore size changes in GelMA:HAMA(9.25:0.75) and GelMA:HAMA(8.75:1.25) show that there is an inhomogeneity in network crosslinking between different compositions. This may be attributed to droplet microfluidics and viscoelastic behavior changes in different compositions. It has been observed that the flow fields inside the droplets produced with droplet microfluidics are highly sensitive to material properties. [73] Furthermore, this pore size gradient, an indicator of the crosslinking density gradient, has been observed in PNiPAM microgels produced with emulsion copolymerization.[74, 75] It is also known that increasing HAMA concentration also alters the mechanical properties, increasing Young's modulus and storage modulus. The highly viscous nature of HA, coming from its large size, enables these profiles.[66, 19] In our case, increasing the HAMA concentration most likely affected both the flow fields and polymerization kinetics, resulting in homogeneous polymer distribution in low HAMA concentrations but a gradient in higher concentrations. This concurrently affects the degradation profiles. Degradation of biomaterials typically follows two modes: surface erosion or bulk erosion. [76]With any of the compositions, the degradation trend was a combination of both but one overpowered the other with changing GelMA:HAMA concentrations. With low HAMA concentrations, bulk erosion was more prominent, and most likely, the less densely crosslinked network and uniform pore structure enabled uniform and fast diffusion of the enzymes. As HAMA concentration was increased to 1%, both degradation modes seemed to be in balance, evidenced by the size decrease and increment in the transparent appearance. With HAMA 1.25%, on the other hand, surface erosion was more prominent up to a certain point. The larger pore size on the outer perimeter compared to the center made it easier for enzymes to degrade the surface, although still slower than lower HAMA concentrations, causing surface erosion. As the outer perimeter degraded and the core was left, the degradation mode switched to bulk erosion with less change in volume, complemented by increased transparency. The surface topology changes accompanying these processes also carry importance for reprogramming the cells, which are quite sensitive to grooves and structural cues. [77] The topography changes were more prominent in increased

HAMA concentrations, which confirms the balance between the diffusivity of enzymes and polymer network crosslink density. Furthermore, groove formation indicates the difference between GelMA and HAMA's degradation speeds. As GelMA degrades faster, the remaining HAMA polymers may be responsible for creating the microstructures.

The mechanical properties of the microgels are highly affected by the network formation as well. Before degradation, the stiffness of microgels was 60 kPa for GelMA:HAMA(8.75:1.25), 42 kPa for GelMA:HAMA(9:1), and 32 kPa for GelMA:HAMA(9.25:0.75), which align well for soft tissue engineering applications.[84] Furthermore, up to the second hour of degradation, GelMA:HAMA(9:1) and GelMA:HAMA(9.25:0.75) microgels showed strain stiffening behavior, which disappeared afterward. Strain stiffening is mainly observed in tissues regularly subjected to load or strain, such as tendons, skin, arteries, and heart. This phenomenon is a result of the fibril structures like collagen, fibrin, and elastin. [78, 79] At low strains, these fibers can bend, but at high strains, they stretch and align. Hyaluronic acid, on the other hand, makes flexible polymer structures, unable to show a strain stiffening response. It has been shown that decreasing the collagen amount delays the strain stiffening response in interpenetrating networks of collagen and hyaluronic acid.[80] Although our networks are copolymer, not interpenetrating, similar behavior is observed. Increasing HAMA concentration appears to disable GelMA fibers from aligning and stiffening the overall network. Within the presence of enzymes, this observation disappears after the second hour. Indicating that GelMA degradation causes the stiffening ability to disappear. Another observation that is directly related to the observed network heterogeneity was the stiffness change profile of GelMA:HAMA(8.75:1.25). A slight decrease in the first hour, followed by a rapid drop and a plateau, shows that the overall denser network initially resists degradation, but as the outer large porous section degrades, and the inner, denser and more uniform network remains, degradation follows a steady trend. The steady and gradual degradation trend is already present in lower HAMA concentrations, a result of a more homogeneous network, where the trends only depend on crosslink density. An interesting outcome was the stiffness of all compositions approximating the same value. This result, combined with

volume change and morphology change observations, proves that estimating the network's momentary status is challenging. How fast the enzymes diffuse in and act on their substrates, the crosslink densities, and uniformity contribute to this multi-parameter complex problem. It should also be argued that, although the stiffness of all compositions stabilized at the same value, their persistence there will be different since GelMA:HAMA(9.25:0.75) degrades completely at the 8^{th} hour and GelMA:HAMA(9:1) degrades faster than GelMA:HAMA(8.75:1.25).

Lastly, we examined the drug release during enzymatic degradation. We selected Rhodamine B, Fluorescein, and Congo Red as model drugs. Rhodamine B is a small molecule positive at low pH and neutral at pH 7.4. Fluorescein is negatively charged, [81, 82]and Congo Red is a molecule used as a model drug that can also interact with collagen.[83, 84] Korsmeyer-Peppas, describing drug release kinetics from polymeric systems, is utilized to evaluate the results. For Rhodamine B and Fluorescein, the expectation was getting a diffusive release profile, while for Congo Red, the degradation is expected to affect the release profile. The low n values for Rhodamine B and Fluorescein indicated Fickian diffusion, and values above 0.45 for Congo Red indicated an enzymatic-induced release. Interestingly, there was no significant difference between GelMA:HAMA compositions in the release of model drugs. Expectation was to have slowed-down release profiles with increasing HAMA concentration, but it seems that this was unrelated. This may be related to the overall pore sizes of microgels and sizes of model drugs.

3.5 Conclusion

Gaining proper control over degradation starts with a thorough understanding of biomaterial behavior under certain conditions. In this work, we examined the physical and mechanical changes in GelMA:HAMA copolymer microgels under the degrative behavior of collagenase and hyaluronidase. We found that a holistic approach to examining the changes in volume, topology, and stiffness is necessary to comment on observed results. Furthermore, the heterogeneity of networks,

crosslink density, enzyme availability, and saturation are important parameters affecting the aforementioned properties. The design of biodegradable materials should be approached with great care and consideration, especially should be made towards a specific application. We believe that this work will contribute to understanding biomaterial degradation, especially microgels, which is very needed considering their increasing popularity.

Bibliography

[1] J. Kim, H. Lee, E.-J. Jin, Y. Jo, B. E. Kang, D. Ryu, and G. Kim, "A microfluidic device to fabricate one-step cell bead-laden hydrogel struts for tissue engineering," *Small*, vol. 18, no. 1, p. 2106487, 2022.

[2] Z. Xiao, T. Wei, R. Ge, Q. Li, B. Liu, Z. Ji, L. Chen, J. Zhu, J. Shen, Z. Liu, *et al.*, "Microfluidic production of zwitterion coating microcapsules with low foreign body reactions for improved islet transplantation," *Small*, vol. 18, no. 29, p. 2202596, 2022.

[3] X. Zhao, S. Liu, L. Yildirimer, H. Zhao, R. Ding, H. Wang, W. Cui, and D. Weitz, "Injectable stem cell-laden photocrosslinkable microspheres fabricated using microfluidics for rapid generation of osteogenic tissue constructs," *Advanced Functional Materials*, vol. 26, no. 17, pp. 2809–2819, 2016.

[4] N. Chai, J. Zhang, Q. Zhang, H. Du, X. He, J. Yang, X. Zhou, J. He, and C. He, "Construction of 3d printed constructs based on microfluidic microgel for bone regeneration," *Composites Part B: Engineering*, vol. 223, p. 109100, 2021.

[5] Z. Zhao, Z. Wang, G. Li, Z. Cai, J. Wu, L. Wang, L. Deng, M. Cai, and W. Cui, "Injectable microfluidic hydrogel microspheres for cell and drug delivery," *Advanced Functional Materials*, vol. 31, no. 31, p. 2103339, 2021.

[6] C. Cai, X. Zhang, Y. Li, X. Liu, S. Wang, M. Lu, X. Yan, L. Deng, S. Liu, F. Wang, *et al.*, "Self-healing hydrogel embodied with macrophage-regulation

and responsive-gene-silencing properties for synergistic prevention of peritendinous adhesion," *Advanced Materials*, vol. 34, no. 5, p. 2106564, 2022.

[7] R. Riahi, A. Tamayol, S. A. M. Shaegh, A. M. Ghaemmaghami, M. R. Dokmeci, and A. Khademhosseini, "Microfluidics for advanced drug delivery systems," *Current Opinion in Chemical Engineering*, vol. 7, pp. 101–112, 2015.

[8] B. Lu, M. D. Tarn, N. Pamme, and T. K. Georgiou, "Fabrication of tailorable ph responsive cationic amphiphilic microgels on a microfluidic device for drug release," *Journal of Polymer Science Part A: Polymer Chemistry*, vol. 56, no. 1, pp. 59–66, 2018.

[9] P. Xue, Y. Wu, N. V. Menon, and Y. Kang, "Microfluidic synthesis of monodisperse pegda microbeads for sustained release of 5-fluorouracil," *Microfluidics and Nanofluidics*, vol. 18, pp. 333–342, 2015.

[10] R. F.-X. Tomasi, S. Sart, T. Champetier, and C. N. Baroud, "Individual control and quantification of 3d spheroids in a high-density microfluidic droplet array," *Cell reports*, vol. 31, no. 8, 2020.

[11] E. Prince, S. Kheiri, Y. Wang, F. Xu, J. Cruickshank, V. Topolskaia, H. Tao, E. W. Young, A. P. McGuigan, D. W. Cescon, *et al.*, "Microfluidic arrays of breast tumor spheroids for drug screening and personalized cancer therapies," *Advanced Healthcare Materials*, vol. 11, no. 1, p. 2101085, 2022.

[12] K. S. McMillan, M. Boyd, and M. Zagnoni, "Transitioning from multi-phase to single-phase microfluidics for long-term culture and treatment of multicellular spheroids," *Lab on a Chip*, vol. 16, no. 18, pp. 3548–3557, 2016.

[13] Y. Zheng, Z. Wu, M. Khan, S. Mao, K. Manibalan, N. Li, J.-M. Lin, and L. Lin, "Multifunctional regulation of 3d cell-laden microsphere culture on an integrated microfluidic device," *Analytical chemistry*, vol. 91, no. 19, pp. 12283–12289, 2019.

[14] K. Y. Lee and D. J. Mooney, "Hydrogels for tissue engineering," *Chemical reviews*, vol. 101, no. 7, pp. 1869–1880, 2001.

[15] J. Li and D. J. Mooney, "Designing hydrogels for controlled drug delivery," *Nature Reviews Materials*, vol. 1, no. 12, pp. 1–17, 2016.

[16] K. T. Nguyen and J. L. West, "Photopolymerizable hydrogels for tissue engineering applications," *Biomaterials*, vol. 23, no. 22, pp. 4307–4314, 2002.

[17] S. R. Caliari and J. A. Burdick, "A practical guide to hydrogels for cell culture," *Nature methods*, vol. 13, no. 5, pp. 405–414, 2016.

[18] D. A. Gyles, L. D. Castro, J. O. C. Silva Jr, and R. M. Ribeiro-Costa, "A review of the designs and prominent biomedical advances of natural and synthetic hydrogel formulations," *European Polymer Journal*, vol. 88, pp. 373–392, 2017.

[19] G. Camci-Unal, D. Cuttica, N. Annabi, D. Demarchi, and A. Khademhosseini, "Synthesis and characterization of hybrid hyaluronic acid-gelatin hydrogels," *Biomacromolecules*, vol. 14, no. 4, pp. 1085–1092, 2013.

[20] S. Xiao, T. Zhao, J. Wang, C. Wang, J. Du, L. Ying, J. Lin, C. Zhang, W. Hu, L. Wang, *et al.*, "Gelatin methacrylate (gelma)-based hydrogels for cell transplantation: an effective strategy for tissue engineering," *Stem cell reviews and reports*, vol. 15, pp. 664–679, 2019.

[21] W. Schuurman, P. A. Levett, M. W. Pot, P. R. van Weeren, W. J. Dhert, D. W. Hutmacher, F. P. Melchels, T. J. Klein, and J. Malda, "Gelatin-methacrylamide hydrogels as potential biomaterials for fabrication of tissue-engineered cartilage constructs," *Macromolecular bioscience*, vol. 13, no. 5, pp. 551–561, 2013.

[22] H. Stratesteffen, M. Köpf, F. Kreimendahl, A. Blaeser, S. Jockenhoevel, and H. Fischer, "Gelma-collagen blends enable drop-on-demand 3d printablility and promote angiogenesis," *Biofabrication*, vol. 9, no. 4, p. 045002, 2017.

[23] A. J. Berger, K. M. Linsmeier, P. K. Kreeger, and K. S. Masters, "Decoupling the effects of stiffness and fiber density on cellular behaviors via an interpenetrating network of gelatin-methacrylate and collagen," *Biomaterials*, vol. 141, pp. 125–135, 2017.

[24] G. Wang, Y. An, X. Zhang, P. Ding, H. Bi, and Z. Zhao, "Chondrocyte spheroids laden in gelma/hama hybrid hydrogel for tissue-engineered cartilage with enhanced proliferation, better phenotype maintenance, and natural morphological structure," *Gels*, vol. 7, no. 4, p. 247, 2021.

[25] C. Onofrillo, S. Duchi, C. D O'Connell, R. Blanchard, A. J. O'Connor, M. Scott, G. G. Wallace, P. F. Choong, and C. Di Bella, "Biofabrication of human articular cartilage: a path towards the development of a clinical treatment," *Biofabrication*, vol. 10, no. 4, p. 045006, 2018.

[26] G. Eke, N. Mangir, N. Hasirci, S. MacNeil, and V. Hasirci, "Development of a uv crosslinked biodegradable hydrogel containing adipose derived stem cells to promote vascularization for skin wounds and tissue engineering," *Biomaterials*, vol. 129, pp. 188–198, 2017.

[27] Y. Ma, X. Wang, T. Su, F. Lu, Q. Chang, and J. Gao, "Recent advances in macroporous hydrogels for cell behavior and tissue engineering," *Gels*, vol. 8, no. 10, p. 606, 2022.

[28] J. Kevin, F. Xu, and T. Hoare, "Structured macroporous hydrogels: Progress, challenges, and opportunities," *Advanced Healthcare Materials*, vol. 7, no. 1, 2017.

[29] A. C. Daly, L. Riley, T. Segura, and J. A. Burdick, "Hydrogel microparticles for biomedical applications," *Nature Reviews Materials*, vol. 5, no. 1, pp. 20–43, 2020.

[30] L. Riley, L. Schirmer, and T. Segura, "Granular hydrogels: emergent properties of jammed hydrogel microparticles and their applications in tissue repair and regeneration," *Current opinion in biotechnology*, vol. 60, pp. 1–8, 2019.

[31] M. Werner, S. B. Blanquer, S. P. Haimi, G. Korus, J. W. Dunlop, G. N. Duda, D. W. Grijpma, and A. Petersen, "Surface curvature differentially regulates stem cell migration and differentiation via altered attachment morphology and nuclear deformation," *Advanced science*, vol. 4, no. 2, p. 1600347, 2017.

[32] L. R. Nih, E. Sideris, S. T. Carmichael, and T. Segura, "Brain transplantation of microporous particle hydrogel after stroke promotes tissue repair and endogenous npc recruitment to the lesion," *Advanced materials (Deerfield Beach, Fla.)*, vol. 29, no. 32, 2017.

[33] E. Sideris, S. Kioulaphides, K. L. Wilson, A. Yu, J. Chen, S. T. Carmichael, and T. Segura, "Particle hydrogels decrease cerebral atrophy and attenuate astrocyte and microglia/macrophage reactivity after stroke," *Advanced therapeutics*, vol. 5, no. 8, p. 2200048, 2022.

[34] Q. Feng, Q. Li, H. Wen, J. Chen, M. Liang, H. Huang, D. Lan, H. Dong, and X. Cao, "Injection and self-assembly of bioinspired stem cell-laden gelatin/hyaluronic acid hybrid microgels promote cartilage repair in vivo," *Advanced Functional Materials*, vol. 29, no. 50, p. 1906690, 2019.

[35] J. Hao, B. Bai, Z. Ci, J. Tang, G. Hu, C. Dai, M. Yu, M. Li, W. Zhang, Y. Zhang, *et al.*, "Large-sized bone defect repair by combining a decalcified bone matrix framework and bone regeneration units based on photocrosslinkable osteogenic microgels," *Bioactive Materials*, vol. 14, pp. 97–109, 2022.

[36] M. Diba, W. A. Camargo, M. Brindisi, K. Farbod, A. Klymov, S. Schmidt, M. J. Harrington, L. Draghi, A. R. Boccaccini, J. A. Jansen, *et al.*, "Composite colloidal gels made of bisphosphonate-functionalized gelatin and bioactive glass particles for regeneration of osteoporotic bone defects," *Advanced Functional Materials*, vol. 27, no. 45, p. 1703438, 2017.

[37] L. V. Le, P. Mohindra, Q. Fang, R. E. Sievers, M. A. Mkrtschjan, C. Solis, C. W. Safranek, B. Russell, R. J. Lee, and T. A. Desai, "Injectable hyaluronic acid based microrods provide local micromechanical and biochemical cues to attenuate cardiac fibrosis after myocardial infarction," *Biomaterials*, vol. 169, pp. 11–21, 2018.

[38] O. Veiseh, J. C. Doloff, M. Ma, A. J. Vegas, H. H. Tam, A. R. Bader, J. Li, E. Langan, J. Wyckoff, W. S. Loo, *et al.*, "Size-and shape-dependent foreign body immune response to materials implanted in rodents and non-human primates," *Nature materials*, vol. 14, no. 6, pp. 643–651, 2015.

[39] C. Shao, J. Chi, L. Shang, Q. Fan, and F. Ye, "Droplet microfluidics-based biomedical microcarriers," *Acta biomaterialia*, vol. 138, pp. 21–33, 2022.

[40] T. Nisisako, "Recent advances in microfluidic production of janus droplets and particles," *Current opinion in colloid & interface science*, vol. 25, pp. 1–12, 2016.

[41] X.-T. Sun, R. Guo, D.-N. Wang, Y.-Y. Wei, C.-G. Yang, and Z.-R. Xu, "Microfluidic preparation of polymer-lipid janus microparticles with staged drug release property," *Journal of colloid and interface science*, vol. 553, pp. 631–638, 2019.

[42] A. J. Engler, S. Sen, H. L. Sweeney, and D. E. Discher, "Matrix elasticity directs stem cell lineage specification," *Cell*, vol. 126, no. 4, pp. 677–689, 2006.

[43] Z. Cao, J. K. Ball, A. H. Lateef, C. P. Virgile, and E. A. Corbin, "Biomimetic substrate to probe dynamic interplay of topography and stiffness on cardiac fibroblast activation," *ACS omega*, vol. 8, no. 6, pp. 5406–5414, 2023.

[44] E. A. Corbin, A. Vite, E. G. Peyster, M. Bhoopalam, J. Brandimarto, X. Wang, A. I. Bennett, A. T. Clark, X. Cheng, K. T. Turner, *et al.*, "Tunable and reversible substrate stiffness reveals a dynamic mechanosensitivity of cardiomyocytes," *ACS applied materials & interfaces*, vol. 11, no. 23, pp. 20603–20614, 2019.

[45] P. Viswanathan, M. G. Ondeck, S. Chirasatitsin, K. Ngamkham, G. C. Reilly, A. J. Engler, and G. Battaglia, "3d surface topology guides stem cell adhesion and differentiation," *Biomaterials*, vol. 52, pp. 140–147, 2015.

[46] D. R. Griffin, W. M. Weaver, P. O. Scumpia, D. Di Carlo, and T. Segura, "Accelerated wound healing by injectable microporous gel scaffolds assembled from annealed building blocks," *Nature materials*, vol. 14, no. 7, pp. 737–744, 2015.

[47] A. K. Gaharwar, I. Singh, and A. Khademhosseini, "Engineered biomaterials for in situ tissue regeneration," *Nature Reviews Materials*, vol. 5, no. 9, pp. 686–705, 2020.

[48] C. Li, C. Guo, V. Fitzpatrick, A. Ibrahim, M. J. Zwierstra, P. Hanna, A. Lechtig, A. Nazarian, S. J. Lin, and D. L. Kaplan, "Design of biodegradable, implantable devices towards clinical translation," *Nature Reviews Materials*, vol. 5, no. 1, pp. 61–81, 2020.

[49] A. G. Cinar, I. Munir, and G. Yesiloz, "Investigating physical properties of hybrid hyaluronic acid and collagen compositions of gelma microgels toward tissue engineering and organ-on-chip applications," *ACS Applied Polymer Materials*, vol. 5, no. 10, pp. 8121–8132, 2023.

[50] E. Hoch, C. Schuh, T. Hirth, G. E. Tovar, and K. Borchers, "Stiff gelatin hydrogels can be photo-chemically synthesized from low viscous gelatin solutions using molecularly functionalized gelatin with a high degree of methacrylation," *Journal of Materials Science: Materials in Medicine*, vol. 23, pp. 2607–2617, 2012.

[51] T. N. Snyder, K. Madhavan, M. Intrator, R. C. Dregalla, and D. Park, "A fibrin/hyaluronic acid hydrogel for the delivery of mesenchymal stem cells and potential for articular cartilage repair," *Journal of biological engineering*, vol. 8, pp. 1–11, 2014.

[52] G. Yesiloz, M. S. Boybay, and C. L. Ren, "Label-free high-throughput detection and content sensing of individual droplets in microfluidic systems," *Lab on a Chip*, vol. 15, no. 20, pp. 4008–4019, 2015.

[53] W. Cui, G. Yesiloz, and C. L. Ren, "Microwave heating induced on-demand droplet generation in microfluidic systems," *Analytical Chemistry*, vol. 93, no. 3, pp. 1266–1270, 2020.

[54] J. W. Nichol, S. T. Koshy, H. Bae, C. M. Hwang, S. Yamanlar, and A. Khademhosseini, "Cell-laden microengineered gelatin methacrylate hydrogels," *Biomaterials*, vol. 31, no. 21, pp. 5536–5544, 2010.

[55] U. S. Madduma-Bandarage and S. V. Madihally, "Synthetic hydrogels: Synthesis, novel trends, and applications," *Journal of Applied Polymer Science*, vol. 138, no. 19, p. 50376, 2021.

[56] Z. Zhan, Z. Liu, H. Nan, J. Li, Y. Xie, and C. Hu, "Heterogeneous spheroids with tunable interior morphologies by droplet-based microfluidics," *Biofabrication*, vol. 14, no. 2, p. 025024, 2022.

[57] M. Chau, M. Abolhasani, H. Therien-Aubin, Y. Li, Y. Wang, D. Velasco, E. Tumarkin, A. Ramachandran, and E. Kumacheva, "Microfluidic generation of composite biopolymer microgels with tunable compositions and mechanical properties," *Biomacromolecules*, vol. 15, no. 7, pp. 2419–2425, 2014.

[58] S. Krishnamoorthy, B. Noorani, and C. Xu, "Effects of encapsulated cells on the physical–mechanical properties and microstructure of gelatin methacrylate hydrogels," *International journal of molecular sciences*, vol. 20, no. 20, p. 5061, 2019.

[59] J. H. Ha, J. H. Lim, J. W. Kim, H.-Y. Cho, S. G. Jo, S. H. Lee, J. Y. Eom, J. M. Lee, and B. G. Chung, "Conductive gelma–collagen–agnw blended hydrogel for smart actuator," *Polymers*, vol. 13, no. 8, p. 1217, 2021.

[60] X. Li, Y. Yang, Y. Fan, Q. Feng, and F. Cui, "Hydrophilicity evaluation of collagen based scaffold optimized by chitin fibres for bone tissue engineering," in *World Congress on Medical Physics and Biomedical Engineering May 26-31, 2012, Beijing, China*, pp. 99–102, Springer, 2013.

[61] M. Vigata, C. Meinert, N. Bock, B. L. Dargaville, and D. W. Hutmacher, "Deciphering the molecular mechanism of water interaction with gelatin methacryloyl hydrogels: Role of ionic strength, ph, drug loading and hydrogel network characteristics," *Biomedicines*, vol. 9, no. 5, p. 574, 2021.

[62] H. Nagano and K. A. To, "Purification of collagenase and specificity of its related enzyme from bacillus subtilis fs-2," *Bioscience, biotechnology, and biochemistry*, vol. 64, no. 1, pp. 181–183, 2000.

[63] I. Mandl, H. Zipper, and L. Ferguson, "Clostridium histolyticum collagenase: its purification and properties," *Archives of Biochemistry and Biophysics*, vol. 74, no. 2, pp. 465–475, 1958.

[64] L. Chung, D. Dinakarpandian, N. Yoshida, J. L. Lauer-Fields, G. B. Fields, R. Visse, and H. Nagase, "Collagenase unwinds triple-helical collagen prior to peptide bond hydrolysis," *The EMBO journal*, vol. 23, no. 15, pp. 3020–3030, 2004.

[65] H. Goodarzi, K. Jadidi, S. Pourmotabed, E. Sharifi, and H. Aghamollaei, "Preparation and in vitro characterization of cross-linked collagen–gelatin hydrogel using edc/nhs for corneal tissue engineering applications," *International journal of biological macromolecules*, vol. 126, pp. 620–632, 2019.

[66] B. Velasco-Rodriguez, T. Diaz-Vidal, L. C. Rosales-Rivera, C. A. García-González, C. Alvarez-Lorenzo, A. Al-Modlej, V. Domínguez-Arca, G. Prieto, S. Barbosa, J. F. A. Soltero Martínez, *et al.*, "Hybrid methacrylated gelatin and hyaluronic acid hydrogel scaffolds. preparation and systematic characterization for prospective tissue engineering applications," *International Journal of Molecular Sciences*, vol. 22, no. 13, p. 6758, 2021.

[67] Z. Pan and L. Brassart, "Constitutive modelling of hydrolytic degradation in hydrogels," *Journal of the Mechanics and Physics of Solids*, vol. 167, p. 105016, 2022.

[68] X. Jia, X. Fan, C. Chen, Q. Lu, H. Zhou, Y. Zhao, X. Wang, S. Han, L. Ouyang, H. Yan, *et al.*, "Chemical and structural engineering of gelatin-based delivery systems for therapeutic applications: A review," *Biomacromolecules*, vol. 25, no. 2, pp. 564–589, 2024.

[69] C. Chircov, A. M. Grumezescu, and L. E. Bejenaru, "Hyaluronic acid-based scaffolds for tissue engineering," *Rom. J. Morphol. Embryol*, vol. 59, no. 1, pp. 71–76, 2018.

[70] H. M. Wyss, T. Franke, E. Mele, and D. A. Weitz, "Capillary micromechanics: Measuring the elasticity of microscopic soft objects," *Soft Matter*, vol. 6, no. 18, pp. 4550–4555, 2010.

[71] T. Kong, L. Wang, H. M. Wyss, and H. C. Shum, "Capillary micromechanics for core–shell particles," *Soft matter*, vol. 10, no. 18, pp. 3271–3276, 2014.

[72] K. Joyce, G. T. Fabra, Y. Bozkurt, and A. Pandit, "Bioactive potential of natural biomaterials: Identification, retention and assessment of biological properties," *Signal transduction and targeted therapy*, vol. 6, no. 1, p. 122, 2021.

[73] M. Li, T. Boulafentis, A. Stathoulopoulos, Z. Liu, and S. Balabani, "Flows inside polymer microfluidic droplets: Role of elasticity," *Chemical Engineering Science*, vol. 278, p. 118887, 2023.

[74] Z. Dai and T. Ngai, "Microgel particles: the structure-property relationships and their biomedical applications," *Journal of Polymer Science Part A: Polymer Chemistry*, vol. 51, no. 14, pp. 2995–3003, 2013.

[75] M. Stieger, W. Richtering, J. S. Pedersen, and P. Lindner, "Small-angle neutron scattering study of structural changes in temperature sensitive microgel colloids," *The Journal of chemical physics*, vol. 120, no. 13, pp. 6197–6206, 2004.

[76] F. Von Burkersroda, L. Schedl, and A. Göpferich, "Why degradable polymers undergo surface erosion or bulk erosion," *Biomaterials*, vol. 23, no. 21, pp. 4221–4231, 2002.

[77] L. V. Le, M. A. Mkrtschjan, B. Russell, and T. A. Desai, "Hang on tight: reprogramming the cell with microstructural cues," *Biomedical microdevices*, vol. 21, pp. 1–17, 2019.

[78] C. F. Guimarães, L. Gasperini, A. P. Marques, and R. L. Reis, "The stiffness of living tissues and its implications for tissue engineering," *Nature Reviews Materials*, vol. 5, no. 5, pp. 351–370, 2020.

[79] A. Karunaratne, S. Li, and A. M. Bull, "Nano-scale mechanisms explain the stiffening and strengthening of ligament tissue with increasing strain rate," *Scientific reports*, vol. 8, no. 1, p. 3707, 2018.

[80] F. Burla, J. Tauber, S. Dussi, J. van Der Gucht, and G. H. Koenderink, "Stress management in composite biopolymer networks," *Nature physics*, vol. 15, no. 6, pp. 549–553, 2019.

[81] A. Wang, Y. Cui, J. Li, and J. C. van Hest, "Fabrication of gelatin microgels by a "cast" strategy for controlled drug release," *Advanced Functional Materials*, vol. 22, no. 13, pp. 2673–2681, 2012.

[82] A. Pepe, P. Podesva, and G. Simone, "Tunable uptake/release mechanism of protein microgel particles in biomimicking environment," *Scientific reports*, vol. 7, no. 1, p. 6014, 2017.

[83] E. I. Yakupova, L. G. Bobyleva, I. M. Vikhlyantsev, and A. G. Bobylev, "Congo red and amyloids: history and relationship," *Bioscience reports*, vol. 39, no. 1, p. BSR20181415, 2019.

[84] S. Yao, H. Liu, S. Yu, Y. Li, X. Wang, and L. Wang, "Drug-nanoencapsulated plga microspheres prepared by emulsion electrospray with controlled release behavior," *Regenerative biomaterials*, vol. 3, no. 5, pp. 309–317, 2016.

Appendix A

Supplementary Data

	2 IU	**1 IU**	**0.5 IU**	**0.1 IU**
1 CDU	2 IU + 1 CDU	1 IU + 1 CDU	0.5 IU + 1 CDU	0.1 IU + 1 CDU
0.5 CDU	2 IU + 0.5 CDU	1 IU + 0.5 CDU	0.5 IU + 0.5 CDU	0.1 IU + 0.5 CDU
0.25 CDU	2 IU + 0.25 CDU	1 IU + 0.25 CDU	0.5 IU + 0.25 CDU	0.1 IU + 0.25 CDU
0.125 CDU	2 IU + 0.125 CDU	1 IU + 0.125 CDU	0.5 IU + 0.125 CDU	0.1 IU + 0.125 CDU

Table A.1: Tested enzyme combinations and concentrations on microgels

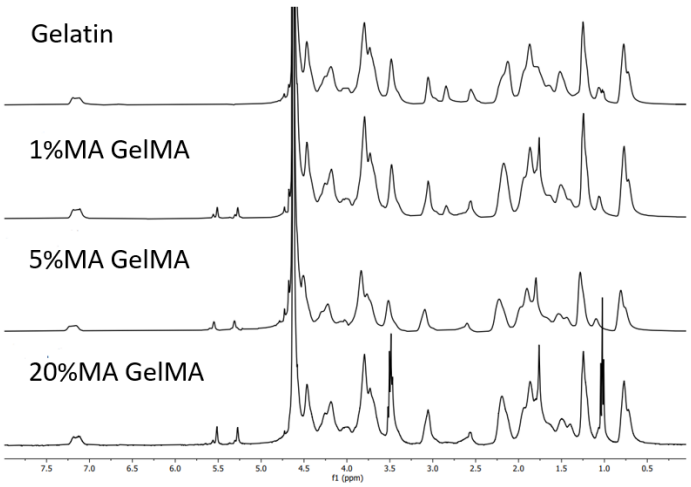

	Degree of Methacrylation (DM)
1%MA GelMA	%55.8
5%MA GelMA	%80
20%MA GelMA	%77.7

Figure A.1: NMR spectra of Gelatin and GelMA synthesized with 1%, 5% and 20%MA and corresponding DM values.

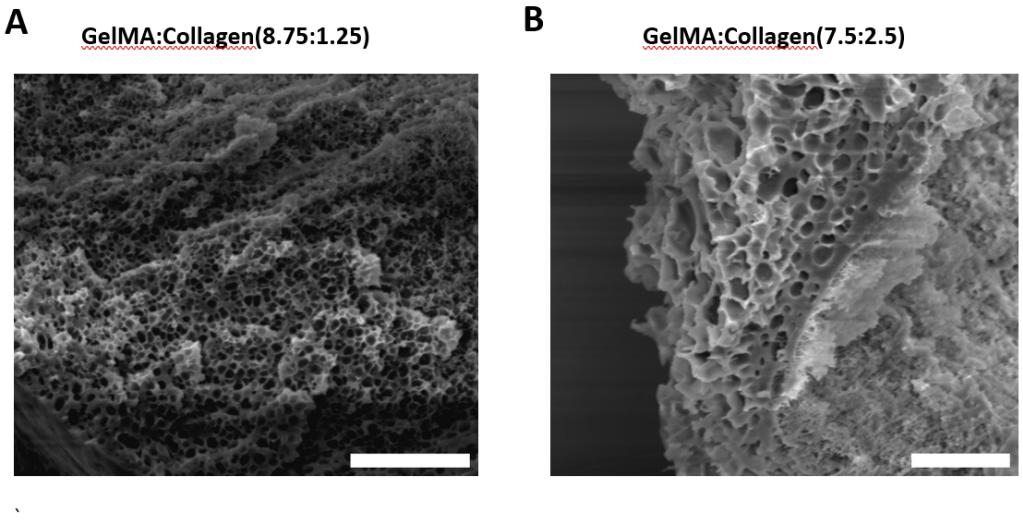

Figure A.2: SEM images of GelMA:Collagen(8.75:1.25)(A) and GelMA:Collagen(7.5:2.5)(B). Scale bars 5μm.

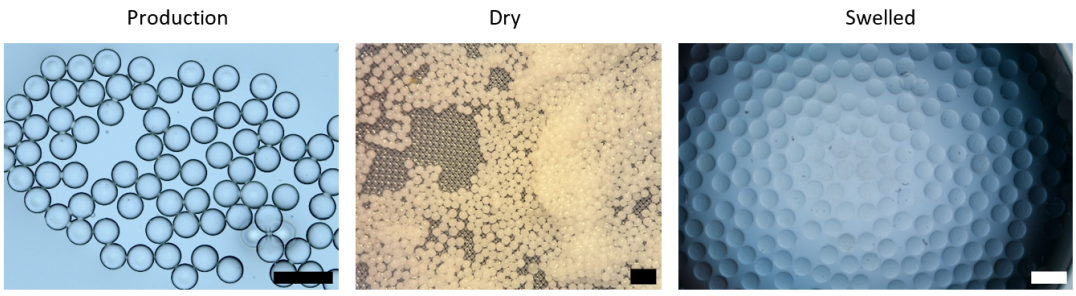

Figure A.3: Microgels right after production, dry and swelled. Scale bars 500 μm